Bachelor's Thesis

Development of Biodegradable Carrageenan-Based Composite Laminate Films with Enhanced Barrier Properties against Oxygen, Water Vapor, and UV Radiation

Department of food Engineering,

College of Engineering, Mokpo National University

Seul-Bi Lee

Bum-Soo Shin

Se-Young Na

Sun Choi

Se-Mi Mun

Supervised by Professor Jae-Young Her

February 2026

Development of Biodegradable Carrageenan-Based Composite Laminate Films with Enhanced Barrier Properties against Oxygen, Water Vapor, and UV Radiation

Department of food Engineering,
College of Engineering, Mokpo National University

Seul-Bi Lee
Bum-Soo Shin
Se-Young Na
Sun Choi
Se-Mi Mun
Supervised by Professor Jae-Young Her

A dissertation submitted in partial fulfillment of
the requirements for the
Bachelor of Science in Food Engineering

Committee in Charge :

Hyun-Jun Lee _____

Jae-Young Her _____

February 2026

Contents

ABSTRACT

CHAPTER 1 Introduction ····· **1**

CHAPTER 2 Materials and Methods ····· **6**

1. Materials ····· 6
2. Preparation of Carrageenan-Based Oxygen-Barrier Composite Films ····· 6
3. Oxygen permeability (OP) ····· 9
4. Water vapor permeability (WVP) ····· 9
5. Measurement of light transmittance ····· 10
6. Surface color measurement ····· 10
7. Mechanical Properties ····· 10
8. Scanning electron microscopy (SEM) ····· 11
9. Potential Application for Oil Packaging ····· 11
10. Statistical analysis ····· 12

CHAPTER 3 Results and Discussion ····· **13**

1. Optimization of oxygen barrier properties in carrageenan-based composite films ····· 13
2. Characterization of PLA/PBAT composite films as water-vapor barrier layers ····· 17
3. Barrier and mechanical performance of bilayer packaging films ····· 21
   1) Scanning electron microscopy analysis ····· 21
   2) Evaluation of oxygen and water vapor permeability ····· 23
   3) Light transmittance and color properties ····· 26
   4) Tensile properties of bilayer films ····· 29

4. Structural and chemical characterization of composite and bilayer films (XRD and FTIR) ····· 31
1) X-ray diffraction (XRD) analysis ····· 31
2) Fourier-transform infrared sprctroscopy (FTIR) analysis ····· 33
5. Food application test: lipid oxidation stability assessed by peroxide value (POV) ····· 36
6. Lipid oxidation kinetics ····· 39

CHAPTER 4 Conclusion ····· 42

References ····· 43

Development of Biodegradable Carrageenan-Based Composite Laminate Films with Enhanced Barrier Properties against Oxygen, Water Vapor, and UV Radiation

Seul-Bi Lee, Bum-Soo Shin, Se-Young Na, Sun Choi, Se-Mi Mun

Department of food Engineering,
College of Engineering, Mokpo National University
(Supervised by Professor Jae-Young Her)

(Abstract)

Recently, interest in developing high-performance biodegradable packaging materials to replace conventional petroleum-based synthetic plastics has rapidly increased due to growing environmental concerns. Carrageenan films exhibit excellent oxygen barrier properties but are susceptible to moisture, while PLA/PBAT blend films show good moisture barrier properties but lack sufficient oxygen barrier performance. To overcome the limitations of these single materials, this study manufactured a bilayer film by combining a carrageenan-based composite film with a PLA/PBAT blend film to optimize the overall barrier characteristics.

In this study, the $CT^{1}M^{3}$ film, prepared by incorporating 1% titanium dioxide (TiO

$_2$) and 3% microcrystalline cellulose (MCC) into carrageenan, was fabricated as the oxygen barrier layer. The L^7B^3 film, a blend of PLA and PBAT at a 7:3 ratio, was used as the moisture barrier layer, ultimately developing the CT1M3/L7B3 laminate film.

The experimental results showed that the CT^1M^3/L^7B^3 bilayer film under optimal conditions exhibited a very low Oxygen Permeability (OP) of 0.191 ± 0.003 $cc/m^2 \cdot day$, demonstrating excellent oxygen barrier performance. Furthermore, the Water Vapor Permeability (WVP) was 0.258 ± 0.069 x 10^{-9} $g \cdot m/m^2 \cdot Pa \cdot s$, confirming its role as an effective moisture barrier. The CT^1M^3/L^7B^3 bilayer film, combining these two layers, achieved simultaneous barrier properties against both oxygen and moisture through the synergy of each layer's advantages. Additionally, the incorporation of TiO_2 and MCC showed a synergistic effect that further strengthened the film's mechanical properties and barrier characteristics.

In conclusion, the CT^1M^3/L^7B^3 bilayer film developed in this study compensates for the drawbacks of existing biodegradable films and achieves superior barrier performance. It confirms its high potential as an eco-friendly food packaging material capable of extending the shelf life of food products requiring protection against rancidity (oxidation) and moisture absorption.

CHAPTER 1 Introduction

1. Introduction

Packaging materials have become an essential component of the modern food industry, playing a critical role in maintaining product freshness and extending shelf life (1,2). During storage and distribution, food products are exposed to various environmental factors, among which oxygen is a major cause of quality deterioration due to its role because of its involvement in oxidative reactions (3,4,5). Therefore, developing packaging materials capable of effectively controlling oxygen permeability is essential (6,7). Among currently used high-barrier materials, ethylene-vinyl alcohol copolymer (EVOH), polyvinylidene chloride (PVDC), and aluminum-deposited films are widely applied due to their excellent oxygen and moisture barrier properties (8). EVOH, which is frequently used as a core barrier layer in multilayer packaging, exhibits very low oxygen permeability under dry conditions because of its high crystallinity and dense hydrogen-bonded network (9,10). However, its barrier performance deteriorates sharply at elevated relative humidity, as water molecules penetrate the polymer matrix, disrupt intermolecular interactions, and increase chain mobility, so additional protective layers are often required, complicating the structure and increasing production costs (10,11). PVDC has also been extensively used as a coating or barrier layer because it combines good oxygen and water vapour barrier properties with reasonable processability, but its chlorine-based backbone raises serious concerns regarding the emission of hazardous compounds during incineration and the generation of problematic chlorinated residues in recycling streams, leading to regulatory and industrial pressure to reduce its use (12). Aluminum-deposited films provide excellent barrier properties against oxygen, water vapour, and light owing to the presence of a continuous metallic layer, and are therefore used for highly sensitive products (13). However, the vacuum deposition process is energy-intensive and costly, and the resulting multilayer structures are difficult to recycle because they

cannot be easily separated into individual components (14). In addition, the metallic nature of these films makes them incompatible with microwave heating, which restricts their use in high-value ready-to-heat or convenience foods that require direct microwaving. Since these materials are primarily synthetic polymer-based, concerns regarding environmental sustainability are increasing (15). The excessive use of plastic packaging and the limited effectiveness of current disposal methods are contributing to serious environmental issues (16,17,18). Consequently, despite their superior barrier performance, these materials, which are primarily synthetic polymer-based, are increasingly viewed as unsustainable solutions in the context of modern packaging requirements (11,14,19).

Concerns regarding plastic waste are especially prominent in the packaging sector. Food packaging commonly relies on materials such as polystyrene (PS), polypropylene (PP), polyethylene (PE), and multilayer laminated films (20,21,22). However, the recyclability of these materials remains limited. In particular, laminated films, which are widely used in the food industry, incorporate interlayer adhesives to maintain their heterogeneous structures (19,23). This design makes mechanical separation challenging, and the distinct melting temperatures of the individual layers prevent remelting, thereby hindering recycling (23,24). Black plastics made from PE and PP further exacerbate this issue, as their dark coloration interferes with detection by optical sorting systems, resulting in low recycling rates (25). As a consequence, the majority of unrecycled plastic packaging is either landfilled or incinerated, contributing to environmental contamination, microplastic accumulation, and greenhouse gas emissions (26,27). Approximately 40% of global plastic production is used for food packaging, yet a substantial portion is not recovered and poses risks to ecosystems and human health (28,29,30). These challenges have driven the implementation of stricter regulations and initiatives aimed at transitioning toward a circular economy (31). In response, biodegradable materials have emerged as promising alternatives. Such materials can degrade into benign end products—including carbon dioxide, water, and biomass—reducing plastic waste and associated

environmental burdens (32,33). Moreover, bio-based polymers that integrate biodegradability with additional functionalities such as antimicrobial, antioxidant, or reinforcement properties are gaining considerable attention for advanced food-packaging applications (34,35,36).

Among these biodegradable polymers, several hydrophilic types have been reported to exhibit very good oxygen-barrier performance (11). In particular, water-soluble polysaccharides such as alginate, pectin, pullulan, and carrageenan can form dense hydrogen-bonded networks under dry conditions (37,38). This compact structure reduces the free volume and diffusion pathways available to non-polar gases and may therefore lead to low oxygen permeability (39). Alginate- and pectin-based films, for example, have been described as having relatively good oxygen barrier properties but limited water vapour resistance and some degree of brittleness (40,41). Their strong affinity for moisture can promote swelling and plasticization of the polymer matrix at elevated relative humidity, which accounts for this behaviour (42,43). Pullulan films are likewise known for very low oxygen permeability and are often investigated as high-oxygen-barrier coatings (44,45). However, their hydrophilic nature is associated with increased water vapour permeability and a loss of mechanical integrity in humid environments (46). Carrageenan, a linear sulfated polysaccharide extracted from red algae, fits within this group and is regarded as a promising candidate for biodegradable food packaging owing to its good film-forming ability, non-toxicity, and natural origin (47,48). Similar to other hydrophilic polysaccharides, neat carrageenan films readily absorb moisture, and the resulting matrix swelling and plasticization tend to deteriorate water vapour barrier properties and mechanical stability, particularly under fluctuating relative humidity (49,50). In contrast, many hydrophobic biodegradable polyesters, such as polylactic acid (PLA) and poly(butylene adipate-co-terephthalate) (PBAT), have relatively low polarity and more densely packed non-polar chains (51,52). These structural features generally restrict their interactions with water molecules and can yield lower and less humidity-sensitive water vapour permeability, even though their oxygen barrier

performance is often inferior to that of hydrophilic polysaccharide films (53). PLA, a thermoplastic polymer derived from renewable resources such as corn starch and sugarcane, offers high transparency, good processability, and suitable heat-sealability for packaging applications (54). However, its relatively high crystallinity and rigid chain structure result in pronounced brittleness and low elongation at break (55,56). PBAT, a petroleum-based yet biodegradable aliphatic–aromatic polyester, provides high extensibility, tear resistance, and flexural durability, thereby partially compensating for the brittleness and low ductility of PLA when the two polymers are blended (57,58). Overall, these reported trends suggest that hydrophilic polysaccharide-based films, including those derived from alginate, pectin, pullulan, and carrageenan, are generally more effective oxygen barriers but more sensitive to moisture (11). By contrast, polyester-based films such as PLA/PBAT blends tend to offer better resistance to water vapour but less effective oxygen barrier performance (59,60). This contrast has motivated the exploration of multilayer structures in which a polysaccharide-rich layer contributes primarily to oxygen barrier performance and a polyester-rich layer contributes mainly to moisture barrier properties and mechanical reinforcement as one possible design strategy for high-barrier biodegradable packaging (61,62).

To further enhance these outstanding features, the structural design and material capabilities of adhesive films are designed to be rich and versatile (61,63). One common strategy is to reinforce a high-barrier or high-density chip matrix (64,65). Cellulose-based nano-additives include MCC(microcrystalline cellulose) and CMF(cellulose microfibril), graphene-based materials such as Graphene Oxide, Graphene Nanoplatelet/metal-inorganic nano-fillers such as Graphene Oxide, and TiO_2(titanium dioxide) (66,67,68). Among the various additives, we attempted to reinforce the film matrix using MCC and TiO_2. MCC is a crystalline material obtained through acid hydrolysis of naturally occurring cellulose. It is colorless, odorless, non-toxic, and biodegradable and is edible (69,70). MCC possesses excellent mechanical properties, thermal stability, and bonding potential, making it suitable for

structural frame construction in special food applications (71,72). In fact, Park et al. (2024) demonstrated that a carrageenan film containing MCC showed greatly enhanced UV-blocking ability, oxygen barrier properties, thermal stability, and mechanical performance (71). TiO_2 is another additive considered safe for food contact (73). TiO_2 acts as a pathogen adsorbent and propagator, and has photocatalytic activity that can inactivate various pathogen groups (74). When TiO_2 is added to a polymer film, it enhances structural stability through hydrogen bonding, improves mechanical strength and thermal resistance, and acts as an impermeable particle that blocks gas diffusion pathways, thereby improving oxygen barrier performance (75,76). In a study supporting this, Shaili (2015) demonstrated that TiO_2 can serve as a catalyst in hydrogen polysaccharide-based films (75).

To date, research on carrageenan-based composite films incorporating both TiO_2 and MCC remains limited, and a systematic analysis of their structural and barrier properties is still lacking. Furthermore, for biodegradable polymer-based films to be applied in practical food packaging systems, not only mechanical stability and functional performance but also processability must be considered. Therefore, this study aims to enhance the structural integrity and barrier functionality of carrageenan films through the incorporation of TiO_2 and MCC, followed by lamination with a PLA/PBAT blend film. To comprehensively evaluate the performance of the developed multilayer films, we measured their thickness, tensile strength, oxygen and water vapor permeability, light transmittance, and Hunter color values. In addition, to assess antioxidant protection, storage experiments were conducted using sunflower oil, and environmental compatibility was examined through a biodegradability test under soil burial conditions. This multilayer approach is intended to overcome the limitations of single bio-polymer films, develop high-performance biodegradable films suitable for real-world packaging applications, and evaluate their potential for future use.

CHAPTER 2 Materials and Methods

1. Materials

In this study, κ-carrageenan was obtained from MSC Co., Ltd. (Yangsan-si, Gyeongsangnam-do, Korea). Microcrystalline cellulose (MCC; Avicel® PH-101, particle size ~50μm) was purchased from Supelco, Sigma-Aldrich (Ireland). Titanium(IV) oxide (anatase type, ≥98.0%purity; TiO_2 = 79.88%) was supplied by Daejung Chemicals & Metals Co., Ltd. (Siheung-si, Gyeonggi-do, Korea). Poly(butylene adipate-co-terephthalate) (PBAT; Ecoflex® F Blend C1200, BASF, Germany) and poly(L-lactic acid) (PLA; Biomer® L9000, weight-average molecular weight≈200 kDa, Biomer Inc., Germany) were dried in a dry oven at 50 °C for at least 48 h prior to use. Chloroform ($CHCl_3$) and glycerol were also obtained from Daejung Chemicals & Metals Co., Ltd. (Siheung-si, Gyeonggi-do, Korea). Potassium iodide (KI) was purchased from Samchun Pure Chemical Co., Ltd. (Seoul, Korea). Sodium thiosulfate standard solution (0.01 N), acetic acid(glacial), and corn starch (used as an indicator) were purchased from Daejung Chemicals & Metals Co., Ltd. (Siheung-si, Gyeonggi-do, Korea). Sunflower oil was obtained from Plus Alpha Trading Co., Ltd. (Seoul, Korea). All chemicals were used as received unless otherwise stated.

2. Preparation of Carrageenan-Based Oxygen-Barrier Composite Films-

Carrageenan-based composite films were prepared using the solution casting method. Based on 3 g of κ-carrageenan, microcrystalline cellulose (MCC; 1, 3, and 5 wt%) and titanium dioxide (TiO_2; 1, 3, and 5 wt%) were dispersed in 100 mL of distilled water. The dispersion was homogenized for 15 min using a high-speed homogenizer (HG-15A, Daihan Scientific, Korea), followed by ultrasonic treatment in

pulse mode at 27% intensity for 10 min (10 sec on /5 sec off) (Model 550, Branson Ultrasonics Corp., USA).

Subsequently, 1.2 g of glycerol was added as a plasticizer, and the solution was stirred for 20 min using a magnetic stirrer. The mixture was then heated to 85°C and stirred at 750 rpm until complete dissolution of the κ-carrageenan. The temperature and stirring speed were reduced to 75°C and 200 rpm, respectively, and the solution was gently stirred for 20 min to remove entrapped air bubbles.

Separately, PLA/PBAT blend (7:3 w/w; total 2 g) was dissolved in 80 mL of chloroform ($CHCl_3$) with continuous magnetic stirring, and cast onto a Teflon-coated glass plate to form the substrate layer. The cast film was dried under ambient conditions (30 ± 2°C, 17 ± 2% RH) for 24 h. After drying, a circular mold was placed on the PLA/PBAT film, and the prepared carrageenan/MCC/TiO_2 solution was poured over it to form the top layer. The multilayer films were dried under the same ambient conditions for 48 h.

The resulting films were carefully peeled off and conditioned in a temperature–humidity chamber (JSTH-150CP, JSR Ltd., Korea) at 25°C and 50% RH for 48 h before characterization. Figure 1 schematically illustrates the film fabrication process.

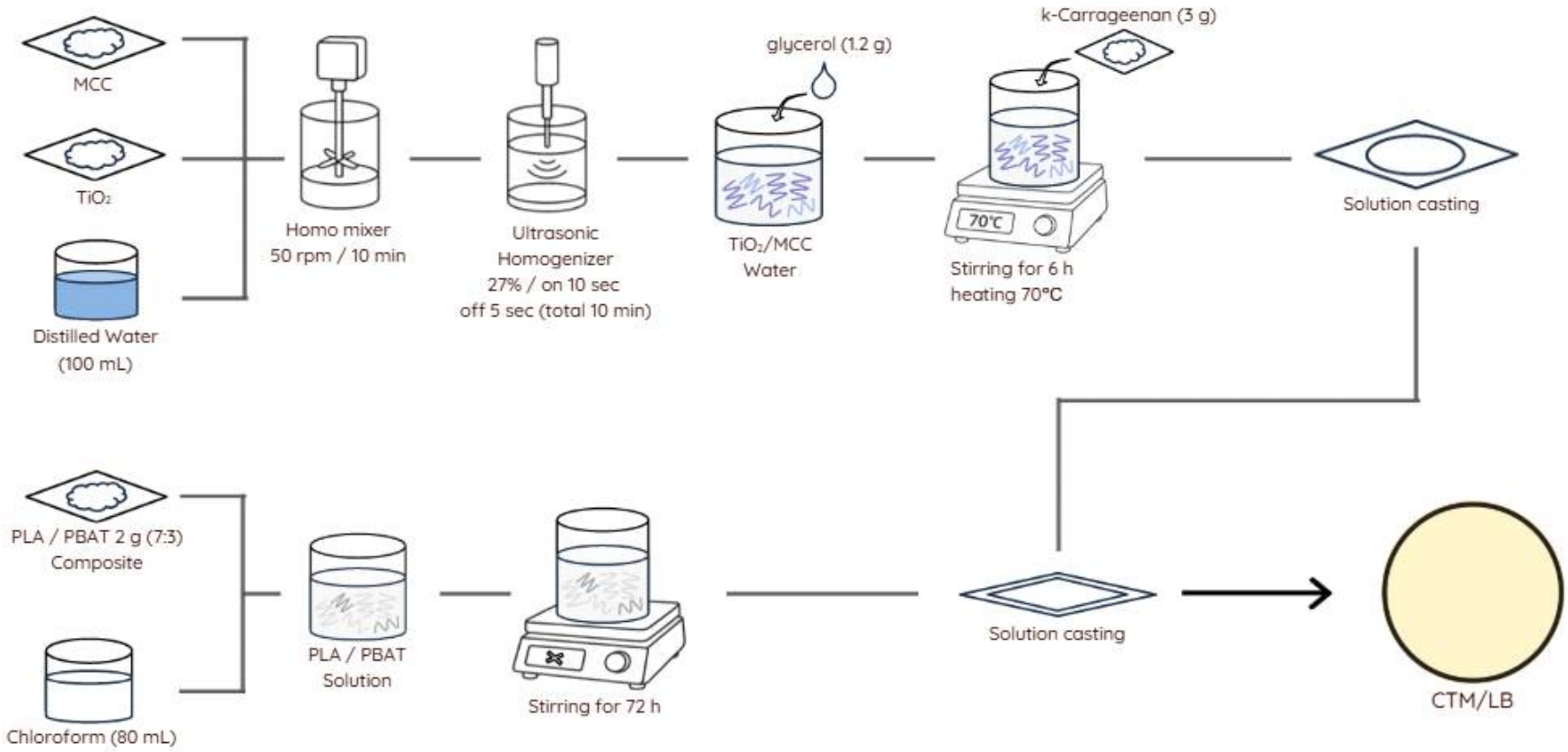


Fig 1. Schematic illustration of the fabrication process for carrageenan-based composite films and CTM/LB multilayer films by solution casting.

3. Oxygen permeability (OP)

Oxygen permeability (OP) was evaluated in accordance with ASTM D3985–05 using a Mocon Oxtran 2/22 system (Minneapolis, USA). The instrument, equipped with a Coulox® colorimetric detector and WinPerm™ software, was operated with films mounted in diffusion cells. Measurements were carried out at 23°C, under 50% relative humidity, and a pressure of 101,325 Pa, with pure oxygen (100%) serving as the testing gas. The OP values were determined from the steady-state oxygen transmission rate (OTR) and adjusted based on film thickness, and results were expressed in $cm^3/m^2 \cdot day$.

4. Water vapor permeability (WVP)

The water vapor transmission rate (WVP) of each film was measured using the ASTM E96-95 standard method. For experimental preparation, the film was cut into 7.5 cm × 7.5 cm sizes and stored in a thermo-hygrostat (JSTH-150CP, JSR Ltd., South Korea). The cut film was placed between a water vapor transmission cup (2.5 cm × 6.8 cm) containing 18 mL of distilled water and a lid, and sealed with four screws. The weight loss was measured at 1-hour intervals for 8 h in a thermo-hygrostat maintained at 25°C and 50% relative humidity. The water vapor shear rate (WVTR) was calculated from the slope calculated from the curve based on the weight loss of the moisture permeability cup, and the WVP was calculated using the following equation:

$$WVP=((WVTR \times t))/\Delta p$$

In the formula, t is the thickness of the film (m), and Δp is the difference in water vapor pressure permeating the film (Pa).

5. Measurement of light transmittance

Light transmittance of each film was measured using a UV-visible spectrophotometer (UV-3600i Plus, Shimadzu, Kyoto, Japan). The films were cut into uniform pieces (2 cm × 3 cm) before measurement. The scanning was performed at very low speed, and the transmittance was recorded at 50 nm intervals over the wavelength range of 200–800 nm.

6. Surface color measurement

The surface colors of the films were measured using a CR-400 Chromaticity meter (Konica Minolta Inc., Osaka, Japan). The overall color difference (ΔE) was calculated based on a white standard plate (L^* = 93.00, a^* = 0.44, b^* = 4.43). Measurements were taken at three random locations throughout the film range, and ΔE was calculated using the following formula:

$$\Delta E = [(\Delta L^*)^2 + (\Delta a^*)^2 + (\Delta b^*)^2]^{0.5}$$

The Hunter color values (L^*, a^*, b^*) were obtained by averaging three measurements, and the differences from the standard plate were expressed as ΔL*, Δa*, and Δb*.

7. Mechanical Properties

Mechanical properties, including tensile strength (TS), elongation at break (E), and elastic modulus (EM), were evaluated using a universal testing machine (UTM, Model 5565, Instron Engineering Corp., USA) in accordance with ASTM D882-88. Film specimens were cut into strips (25 mm × 150 mm), and the initial grip separation was set at 50 mm. The crosshead speed during testing was maintained at 50 mm/min.

Tensile strength (TS) was calculated using the following equation:

$$TS = \frac{F}{A}$$

where $F$is the maximum tensile force (N) and $A$is the cross-sectional area of the film (m^2).

Elongation at break (E) was calculated as:

$$E = (\frac{E_f - E_0}{E_0}) X 100$$

where $E_0$is the initial gauge length (50 mm), and E_f is the length at break.

Elastic modulus (EM) was determined from the slope of the initial linear portion of the stress–strain curve and expressed in GPa.

8. Scanning electron microscopy (SEM)

The structure of C-T^1M^3 film, L^7B^3 film, and their bilayer film (C-T^1M^3/L^7B^3) and microparticle was observed using a field emission electron microscope (FE-SEM, S-4800, Hitachi Co. Ltd., Japan). Each film sample was cut into small square pieces (1 cm × 1 cm) and mounted on an aluminum stub using conductive carbon tape. The samples were sputter-coated with a thin platinum layer for 2 min prior to observation. SEM micrographs were recorded at magnifications of 1000 ×under an accelerating voltage of 3 kV.

9. Potential Application for Oil Packaging

Sunflower seed oil was dispensed into a 100 mL beaker, and the corresponding film samples were placed on the top of the beaker as a cover. The samples were stored under normal storage conditions at 28°C for 70 days.

The method used to measure peroxide formation during the sunflower seed oil storage test is described below.

Approximately 1.0 g of the sample was weighed and placed in a 250 mL Erlenmeyer flask. 50 mL of a mixture of acetic acid and chloroform (3:2, v/v) was added to completely dissolve the sample. Immediately, 1 mL of a saturated potassium iodide (KI) solution was added, the flask was capped, and gently stirred for 30 second. The flask was kept in the dark for 10 minute to complete the reaction between hydrogen peroxide and iodide. After the reaction, 1 mL of a 1% starch solution was added as an indicator. The liberated iodine was immediately titrated with a standard 0.01 N sodium thiosulfate ($Na_2S_2O_3$) solution. The titration was continued until the dark blue color completely disappeared and became colorless, indicating complete reduction of iodine to iodide (I-).

The POV was calculated according to the following equation:

$$POV = ((V_1-V_0)\times F\times 0.01)/S$$

10. Statistical analysis

All results are reported as the mean ± standard deviation (SD) based on three to five independent replicates. Statistical analyses were performed using SPSS (SPSS Inc., Chicago, IL, USA). Differences among groups were assessed by one-way ANOVA, and multiple comparisons were conducted using Duncan's multiple range test. Statistical significance was set at $p < 0.05$. Kinetic parameters obtained from the lipid-oxidation model (rate constant, k, and area under the curve, AUC) were evaluated using the same statistical procedure.

CHAPTER 3 Results and Discussion

1. Optimization of oxygen barrier properties in carrageenan-based composite films

Oxygen permeability quantifies the amount of oxygen gas passing through a unit area per unit time and serves as a critical parameter for evaluating the oxygen barrier properties of packaging systems (61). Table 1 presents the oxygen permeability values of neat carrageenan film and composite films prepared with varying ratios of TiO_2 and MCC, including CT^1, CT^3, CT^5, CM^1, CM^3, CM^5, and their combinations. The neat carrageenan film, serving as the negative control, exhibited an oxygen permeability of 1.669 ± 0.485 cc/m²·day, whereas the commercial LID film used as the positive control showed a significantly lower value of 0.305 ± 0.018 cc/m²·day. The negative control demonstrated approximately 447% higher oxygen permeability compared to the positive control, with this difference being statistically significant ($p < 0.05$). The incorporation of either MCC or TiO_2 alone substantially reduced the oxygen permeability of carrageenan films compared to the neat film. Films containing MCC at 1%, 3%, and 5% concentrations exhibited oxygen permeability values of 0.611 ± 0.007, 0.606 ± 0.032, and 0.560 ± 0.027 cc/m²·day, respectively, representing reductions of 63.4–66.5% relative to the negative control. Similarly, films incorporating TiO_2 at equivalent concentrations displayed values of 0.342 ± 0.001, 0.314 ± 0.029, and 0.294 ± 0.032 cc/m²·day, respectively, corresponding to reductions of 79.5–82.4%. Both additives significantly improved oxygen barrier properties compared to neat carrageenan film ($p < 0.05$). Composite films containing both TiO_2 and MCC exhibited oxygen permeability values ranging from 0.192 to 0.550 cc/m²·day. Among all formulations, CT^1M^3 demonstrated the lowest oxygen permeability of 0.192 ± 0.009 cc/m²·day, representing an 88.5% reduction compared to the negative control and the highest oxygen barrier

performance across all experimental groups ($p < 0.05$). Notably, the performance of CT^1M^3 exceeded the additive effect of 1% TiO_2 alone with 79.5% reduction and 3% MCC alone with 63.7% reduction, suggesting a synergistic interaction between these two components. The reduction in oxygen permeability can be attributed to the complementary mechanisms of MCC and TiO_2 nanoparticles (77). The hydroxyl groups on MCC surfaces form strong hydrogen bonding networks with carrageenan molecules, resulting in a denser film structure and increased tortuosity of oxygen diffusion pathways (71). Meanwhile, TiO_2 nanoparticles act as impermeable inorganic fillers that reduce the free volume between polymer chains and physically obstruct gas molecule migration, thereby lowering oxygen permeability (75). These findings align with previous studies. Park et al. (2024) reported approximately 75% reduction in oxygen permeability when MCC extracted from pistachio shells was incorporated into carrageenan films. Similarly, Shaili et al. (2015) observed approximately 68% reduction in oxygen permeability upon addition of 3% TiO_2 to starch-based films (71,75). The present study demonstrates that the CT^1M^3 formulation, combining 1% TiO_2 and 3% MCC, achieves optimal balance with an 88.5% reduction in oxygen permeability relative to the negative control. These results confirm that appropriate blending of TiO_2 and MCC at a 1:3 ratio represents an effective strategy for significantly enhancing the oxygen barrier properties of carrageenan films. However, water vapor permeability values across all formulations ranged from 20.967 to 26.700 $\times 10^{-9}$ g·m/m²·Pa·s, showing no statistically significant difference from neat carrageenan film at 20.567 $\times 10^{-9}$ g·m/m²·Pa·s ($p > 0.05$). These values were approximately 1,000-fold higher than that of the positive control at 0.017 $\times 10^{-9}$ g·m/m²·Pa·s, indicating that while TiO_2 and MCC addition effectively improved oxygen barrier properties, it failed to enhance water vapor barrier performance. This limitation is attributed to the abundant hydrophilic functional groups (-OH, $-OSO_3^-$) within the carrageenan polymer chains, which facilitate moisture absorption and permeation. In conclusion, carrageenan composite films with the CT^1M^3 formulation exhibited excellent oxygen barrier properties;

however, their limited water vapor barrier performance restricts their stand alone application as food packaging materials in high-humidity environments. Therefore, lamination with hydrophobic polymer films possessing superior water vapor barrier properties is required. To address this limitation, PLA/PBAT-based composite films were designed as the hydrophobic outer layer of a multilayer packaging system, and their barrier and mechanical properties were subsequently evaluated.

Table 1. Oxygen permeability and water vapor permeability of carrageenan-based composite films with varying TiO_2 and MCC concentrations.

Sample	Oxygen permeability(cc/m^2· day)	WVP(x10^{-9}g·m/m^2·Pa·s)
Neat Carrageenan	1.669±0.485^{f}	2.057±0.067^{b}
Positive control	0.305±0.018^{abc}	0.002±0.001^{a}
CM^1	0.611±0.007^{e}	2.097±0.131^{b}
CM^3	0.606±0.032^{e}	2.397±0.095^{abc}
CM^5	0.560±0.027^{de}	2.223±0.267^{ab}
CT^1	0.342±0.001^{abcd}	2.173±0.087^{ab}
CT^3	0.314±0.029^{abc}	2.403±0.145^{abc}
CT^5	0.294±0.032^{abc}	2.223±0.132^{ab}
CT^1M^1	0.217±0.005^{ab}	2.167±0.080^{ab}
CT^1M^3	0.192±0.009^{a}	2.247±0.360^{ab}
CT^1M^5	0.506±0.005^{cde}	2.303±0.093^{abc}
CT^3M^1	0.227±0.075^{ab}	2.223±0.255^{ab}
CT^3M^3	0.246±0.006^{ab}	2.513±0.376^{bc}
CT^3M^5	0.550±0.029^{de}	2.670±0.151^{c}
CT^5M^1	0.228±0.027^{ab}	2.423±0.310^{abc}
CT^5M^3	0.252±0.031^{ab}	2.380±0.252^{abc}
CT^5M^5	0.448±0.046^{bcde}	2.393±0.197^{abc}

Values are expressed as mean ± standard deviation (n = 3). Different superscript letters within the same column indicate statistically significant differences ($p < 0.05$) by Duncan's multiple range test. CT, carrageenan with TiO_2; CM, carrageenan with MCC; numerical superscripts denote additive concentration (wt%).

2. Characterization of PLA/PBAT composite films as water-vapor barrier layers

To overcome the poor moisture barrier performance of carrageenan-based composite films, PLA/PBAT-based composite films were developed and evaluated as hydrophobic layers within multilayer packaging structures. The mechanical properties of these films are summarized in Table 2. Pure PLA film exhibited relatively high tensile strength but possessed a high elastic modulus and limited elongation at break, indicating its rigid and brittle nature. In contrast, pure PBAT film showed lower tensile strength but a low modulus and high elongation at break, demonstrating its flexible and ductile characteristics. The mechanical properties of the PLA/PBAT blend films (LB) gradually changed depending on the blend composition. As PBAT content increased, the LB films showed decreased tensile strength and modulus, while elongation at break increased compared with pure PLA. Among the tested ratios, the PLA/PBAT 7:3 (L^7B^3) blend exhibited mechanical properties most comparable to those of the optimized CT^1M^3 film. The elastic modulus is a key determinant of interlayer deformation behavior in multilayer structures (78). When adjacent layers possess similar elastic moduli, they deform proportionally under external stress, resulting in a uniform strain distribution across the interface (79). Conversely, when the modulus mismatch is large, the soft layer undergoes excessive stretching while the rigid layer resists deformation, causing stress concentration at the interface and potentially leading to delamination during processing, storage, or humidity fluctuations (79,80). Based on these considerations, L^7B^3 film was selected as the hydrophobic layer for lamination with CT^1M^3. The water vapor barrier performance of the selected L^7B^3 film is presented in Table 3. The water vapor permeability (WVP) of L^7B^3 was 0.336×10^{-9} g·m/m²·Pa·s, which was approximately 98.5% lower than that of CT^1M^3 (22.467×10^{-9} g·m/m²·Pa·s). This value was comparable to that of a commercial high-barrier positive control (0.017×10^{-9} g·m/m²·Pa·s), confirming that L^7B^3 exhibits moisture-barrier performance approaching commercial standards. These

results are attributed to the hydrophobic ester-bond-rich structures of PLA and PBAT, effectively compensating for the intrinsic moisture sensitivity of the hydrophilic $CT^{1}M^{3}$ film. In conclusion, the $L^{7}B^{3}$ film demonstrated mechanical compatibility with $CT^{1}M^{3}$ and excellent moisture barrier properties, making it a suitable candidate for use as the moisture-barrier layer in multilayer packaging. Subsequent analyses were conducted to evaluate the lamination properties of the two films.

Table 2. Mechanical properties of PLA, PBAT, PLA/PBAT blend (LB) films, and CT^1M^3 film.

Sample	Tensile strength(Mpa)	Elastic modulus(Mpa)	Elongation at break(%)
PLA	33.09±0.22^{c}	2028.07±114.84^{e}	5.12±0.92^{a}
L^9B^1	39.28±0.13^{d}	2208.69±274.22^{e}	11.63±9.21^{a}
L^8B^2	35.47±1.07^{cd}	1897.19±663.22^{e}	42.51±13.94^{a}
L^7B^3	24.48±1.59^{b}	1450.71±179.30^{d}	33.58±15.20^{a}
L^6B^4	14.26±0.41^{a}	679.03±44.58^{c}	24.99±3.47^{a}
L^5B^5	13.22±1.40^{a}	566.97±42.90^{bc}	12.87±1.41^{a}
L^4B^6	16.34±0.66^{a}	697.87±124.81^{c}	25.85±7.13^{a}
L^3B^7	13.42±0.89^{a}	243.91±32.55^{ab}	38.95±8.64^{a}
L^2B^8	12.41±0.41^{a}	137.29±10.86^{a}	212.10±66.21^{b}
L^1B^9	14.05±1.45^{a}	104.22±3.43^{a}	324.33±88.83^{c}
PBAT	13.99±2.65^{a}	76.05±3.36^{a}	386.69±180.58^{c}
CT^1M^3	34.44±1.22^{c}	1201.76±18.81^{d}	17.74±1.96^{a}

Different superscript letters within the same column indicate statistically significant differences ($p < 0.05$) by Duncan's multiple range test.

Table 3. Oxygen permeability (OP) and water vapor permeability (WVP) of control, positive control, L^7B^3, and CT^1M^3 films.

Sample	Oxygen permeability(cc/m^2· day)	WVP(x10^{-9}g·m/m^2·Pa·s)
Control (Carr)	1.669±0.485^a	20.567±0.666^b
Positive control	0.305±0.018^b	0.017±0.008^a
L^7B^3	-	0.336±0.006^a
CT^1M^3	0.192±0.009^b	22.467±3.591^b

Values are expressed as mean ± standard deviation (n = 3). Different superscript letters within the same column indicate statistically significant differences ($p < 0.05$) by Duncan's multiple range test.

3. Barrier and mechanical performance of bilayer packaging films

1) Scanning electron microscopy analysis

Figure 2 presents cross-sectional field-emission scanning electron microscopy (FE-SEM) images of CT^1M^3, L^7B^3, and the bilayer film. The CT^1M^3 film formed a uniform and continuous matrix, consistent with the dense and homogeneous microstructure typically reported for hydrophilic polysaccharide-based films (81,82). In contrast, the L^7B^3 film exhibited a heterogeneous morphology characterized by distinct phase-separated domains and intermittent microvoids. This behavior is consistent with previous reports indicating that PLA/PBAT blends are immiscible or partially miscible systems that typically form droplet-matrix or sea-island phase separation structures across various composition ranges (83,84). The laminated bilayer film displayed two distinct yet tightly bonded polymer layers at the interface, forming a stable multilayer structure similar to other biopolymer/PLA-based multilayer systems (85,86). Such multilayer architectures are widely recognized to enhance gas and water vapor barrier properties compared to monolayer films by increasing the effective diffusion path length for permeating molecules, as demonstrated in PLA/protein, PLA/gelatin multilayer films, and carrageenan-based multilayer structures (85,87,88). Therefore, the interfacial morphology observed in this study aligns well with the general mechanism by which multilayer structures enhance mass transfer resistance. Overall, FE-SEM analysis confirms that the three films possess inherently different microstructures. In particular, the laminated CT^1M^3/L^7B^3 film structure offers potential advantages in maintaining the intrinsic properties of each constituent layer while simultaneously enhancing structural stability and barrier performance.

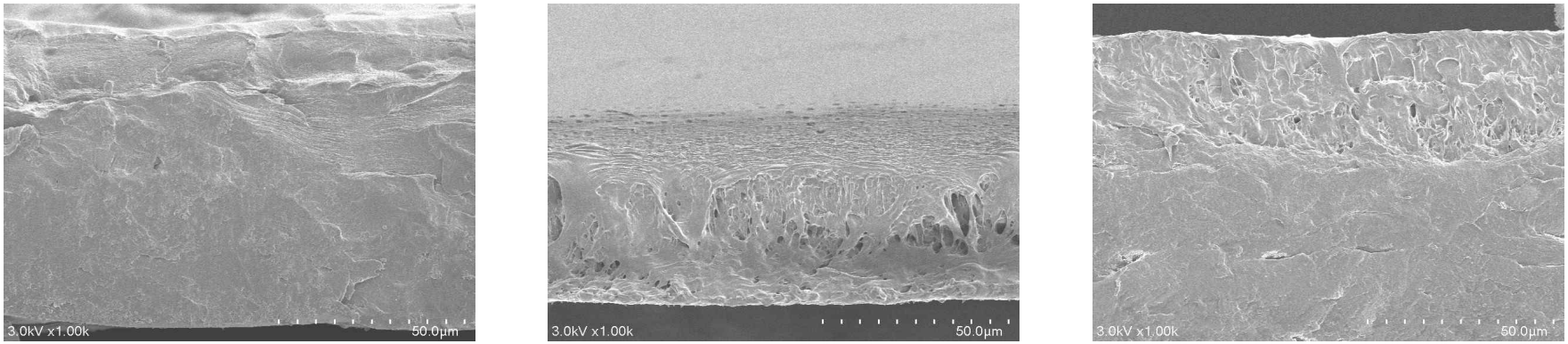


Fig 2. Cross-sectional FE-SEM images of CT^1M^3, L^7B^3, and the laminated CT^1M^3/L^7B^3 film.

2) Evaluation of oxygen and water vapor permeability

The oxygen permeability (OP) and water vapor permeability (WVP) of the selected CT^1M^3 and CT^1M^3/L^7B^3 films are presented in Table 4. The neat carrageenan control film exhibited the highest oxygen permeability of 1.669 ± 0.485 cc/m²·day, confirming its significantly poor oxygen barrier performance. In contrast, the commercial LID film used as the positive control showed a significantly lower value of 0.305 ± 0.018 cc/m²·day. Consistent with the results described above, the carrageenan composite film CT^1M^3 incorporated with 1 wt% TiO_2 and 3 wt% MCC exhibited a substantially reduced oxygen permeability of 0.192 ± 0.009 cc/m²·day, representing an 88.5% reduction compared to the neat carrageenan film. The bilayer film composed of an inner CT^1M^3 layer and an outer L^7B^3 layer demonstrated an oxygen permeability of 0.191 ± 0.003 cc/m²·day, corresponding to an 88.6% reduction relative to the control film. No statistically significant differences in oxygen permeability were observed among the positive control, CT^1M^3, and bilayer films ($p > 0.05$), whereas the neat carrageenan film maintained substantially higher permeability. These results indicate that lamination with the L^7B^3 layer did not compromise the excellent oxygen barrier performance of the optimized carrageenan composite film, and the overall oxygen barrier performance of the bilayer structure is predominantly governed by the CT^1M^3 layer. In contrast, the water vapor permeability results clearly demonstrate that the L^7B^3 outer layer significantly contributes to moisture barrier performance. The neat carrageenan control and CT^1M^3 films exhibited high water vapor permeability values of 20.567 ± 0.666 and 22.467 ± 3.591 × 10^{-9} g·m/m²·Pa·s, respectively, with no statistically significant difference observed between them ($p > 0.05$). This confirms that the addition of TiO_2 and MCC did not improve the inherent moisture barrier properties of the hydrophilic carrageenan matrix. Conversely, the L^7B^3 monolayer film exhibited a substantially lower water vapor permeability of 0.336 ± 0.006 × 10^{-9} g·m/m²·Pa·s, and the bilayer film demonstrated an even lower value of 0.258 ± 0.069 × 10^{-9} g·m/m²·Pa·s.

Neither value showed a statistically significant difference from the commercial LID film at $0.017 \pm 0.008 \times 10^{-9}$ g·m/m²·Pa·s ($p > 0.05$). The water vapor permeability of the bilayer film was approximately 98.7% and 98.9% lower than those of the neat carrageenan and CT^1M^3 films, respectively, representing a reduction of nearly two orders of magnitude. Collectively, these results demonstrate that the bilayer structure successfully combines the functional advantages of both constituent materials. The inner CT^1M^3 layer provides high oxygen barrier performance comparable to the commercial LID film, while the outer L^7B^3 layer effectively compensates for the poor water vapor resistance of carrageenan, achieving water vapor permeability values within the same statistical range as commercial high-barrier films. Therefore, the CT^1M^3/L^7B^3 bilayer film demonstrates potential as a promising high-barrier packaging material for foods sensitive to both oxygen and moisture.

Table 4. Oxygen permeability (OP) and water vapor permeability (WVP) of control, CT^1M^3, L^7B^3, and CT^1M^3/L^7B^3 bilayer films compared with a commercial positive control (LID).

Sample	Oxygen permeability($cc/m^2 \cdot$ day)	WVP($x10^{-9} g \cdot m/m^2 \cdot Pa \cdot s$)
Control (Carr)	1.669 ± 0.485^a	20.567 ± 0.666^b
Positive control(LID)	0.305 ± 0.018^b	0.017 ± 0.008^a
L^7B^3	-	0.336 ± 0.006^a
CT^1M^3	0.192 ± 0.009^b	22.467 ± 3.591^b
CT^1M^3/L^7B^3	0.191 ± 0.003^b	0.258 ± 0.069^a

Values are expressed as mean ± standard deviation (n = 3). Different superscript letters within the same column indicate statistically significant differences ($p < 0.05$) by Duncan's multiple range test.

3) Light transmittance and color properties

The optical transmittance and UV-blocking properties of packaging films play a critical role in determining the photo-oxidative stability and visual quality of packaged foods (89). Table 5 presents the color differences and light transmittance values of each film measured at 280 nm and 660 nm. Pure carrageenan films exhibited relatively high transmittance values of 36.58% at 280 nm and 57.69% at 660 nm, indicating poor UV and visible light barrier performance. In contrast, the positive control film showed transmittance values of only 0.001% at 280 nm and 0.55% at 660 nm, demonstrating nearly complete light-blocking behavior across the measured wavelength range. This result confirms the excellent optical barrier properties of the commercial high-barrier packaging material. The transmittance of TiO_2-containing composite films decreased significantly with increasing TiO_2 concentration ($p < 0.05$). The CT films exhibited transmittance values ranging from 0.002% to 2.65% at 280 nm and from 0.13% to 4.96% at 660 nm. A clear decreasing trend in transmittance was observed as the TiO_2 content increased, which can be attributed to enhanced light scattering and absorption induced by TiO_2 particles dispersed within the film matrix. This UV-shielding mechanism of TiO_2 has also been reported in recent reviews on TiO_2-based food packaging films (74). A similar trend was observed in C-TM films containing both TiO_2 and MCC. Park et al. (2024) reported that MCC extracted from pistachio shells acted as a micro-filler within carrageenan films, densifying the film structure and increasing light diffusion pathways, thereby enhancing UV-blocking performance (71). Consistent with this report, all C-TM films in the present study exhibited significantly lower transmittance at 280 nm compared to pure carrageenan films ($p < 0.05$), along with an overall reduction in transmittance at 660 nm. These results align with the improved UV and visible light barrier properties observed in MCC-containing composite films. The enhanced optical barrier performance can be attributed to the microfibrillar structure of MCC, which introduces irregular light scattering pathways within the film matrix.

Furthermore, the synergistic interaction between MCC and TiO_2 appears to amplify light-blocking efficiency through combined scattering and absorption effects.

The CT^1M^3/L^7B^3 bilayer film exhibited transmittance values of 0.001% at 280 nm and 0.56% at 660 nm, which were comparable to those of the positive control. This indicates nearly complete UV shielding performance. The superior optical barrier behavior of the bilayer structure can be explained by multiple internal reflections and scattering events occurring at the interface between the CT^1M^3 and L^7B^3 layers, which increase the optical path length and effectively suppress overall light transmission through the film.

Color difference analysis further supported these optical changes. Pure carrageenan films exhibited the highest L* value (94.49), indicating a bright and highly transparent appearance. In contrast, films containing TiO_2 showed decreased L* values and increased b* values, resulting in a visually opaque, whitish appearance. This change can be attributed to increased light scattering and reflection caused by TiO_2 particles. Films containing additional MCC exhibited a further decrease in L* values and a significant increase in ΔE values ($p < 0.05$), indicating greater brightness reduction and stronger visual opacity. These color changes were consistent with the reduced transmittance observed at both 280 nm and 660 nm, confirming the effective enhancement of UV and visible light barrier properties. Overall, the combined incorporation of TiO_2 and MCC, along with the application of a multilayer structure, significantly enhanced the UV and visible light shielding performance of carrageenan-based films. These improved optical properties are expected to be beneficial for preventing discoloration and quality deterioration of light-sensitive foods. Therefore, the composite and multilayer film design employing TiO_2 and MCC presents a promising strategy for the practical application of carrageenan-based sustainable packaging materials.

Table 5. Color parameters (L*, a*, b*, ΔE) and light transmittance at 280 and 660 nm of carrageenan-based composite and bilayer films.

Sample	*L**	*a**	*b**	*ΔE*	280nm	660nm
Control	94.489 ± 0.067^{ij}	-0.332 ± 0.011^{f}	4.359 ± 0.070^{a}	-	36.583 ± 2.536^{g}	57.686 ± 4.871^{g}
Positive control	-	-	-	-	0.001 ± 0.002^{a}	0.551 ± 0.024^{a}
CT^{1}M^{3}/ L^{7}B^{3}	93.698± 0.059^{abc}	-0.566 ± 0.234^{abcde}	7.118 ± 0.166^{e}	2.896 ± 0.133^{fgh}	0.001 ± 0.001^{a}	0.559 ± 0.039^{a}
CM^{1}	94.310 ± 0.070^{ghi}	-0.391 ± 0.020^{ef}	4.782 ± 0.198^{ab}	0.467 ± 0.197^{ab}	23.294 ± 1.736^{f}	35.561 ± 3.090^{f}
CM^{3}	94.548 ± 0.099^{ij}	-0.449 ± 0.002^{def}	4.857 ± 0.127^{b}	0.521 ± 0.125^{ab}	13.606 ± 1.826^{e}	21.120 ± 3.306^{e}
CM^{5}	94.636 ± 0.140^{j}	-0.490 ± 0.006^{cdef}	5.019 ± 0.190^{b}	0.711 ± 0.143^{b}	8.641 ± 1.045^{d}	14.410 ± 1.741^{d}
CT^{1}	93.851 ± 0.089^{bcd}	-0.623 ± 0.034^{abcd}	7.634 ± 0.282^{fg}	3.350 ± 0.295^{hi}	2.649 ± 0.519^{c}	4.961 ± 0.782^{c}
CT^{3}	94.119 ± 0.056^{defg}	-0.574 ± 0.058^{bcde}	7.219 ± 0.076^{ef}	2.895 ± 0.076^{fgh}	0.025 ± 0.011^{a}	0.195 ± 0.026^{a}
CT^{5}	94.397 ± 0.312^{huj}	-0.483 ± 0.027^{cdef}	6.482 ± 0.430^{c}	2.147 ± 0.425^{cd}	0.002 ± 0.003^{a}	0.132 ± 0.012^{a}
CT^{1}M^{1}	93.447 ± 0.101^{a}	-0.798 ± 0.008^{a}	7.723 ± 0.029^{g}	3.554 ± 0.014^{i}	1.492 ± 0.292^{b}	3.956 ± 0.515^{c}
CT^{1}M^{3}	93.624 ± 0.025^{ab}	-0.461 ± 0.314^{cdef}	7.419 ± 0.039^{efg}	3.193 ± 0.058^{ghi}	0.768 ± 0.223^{ab}	2.247 ± 0.470^{b}
CT^{1}M^{5}	93.847 ± 0.205^{bcd}	-0.753 ± 0.067^{ab}	7.124 ± 0.483^{e}	2.871 ± 0.518^{fgh}	0.556 ± 0.221^{a}	1.465 ± 0.528^{ab}
CT^{3}M^{1}	93.896 ± 0.170^{bcde}	-0.636 ± 0.069^{abcd}	6.576 ± 0.362^{cd}	2.316 ± 0.394^{cde}	0.022 ± 0.016^{a}	0.213 ± 0.040^{a}
CT^{3}M^{3}	93.878 ± 0.287^{bcde}	-0.614 ± 0.057^{abcd}	6.642 ± 0.526^{cd}	2.383 ± 0.586^{def}	0.021 ± 0.008^{a}	0.208 ± 0.014^{a}
CT^{3}M^{5}	94.174 ± 0.061^{fgh}	-0.666 ± 0.054^{abc}	6.550 ± 0.191^{cd}	2.240 ± 0.186^{cd}	0.009 ± 0.004^{a}	0.175 ± 0.005^{a}
CT^{5}M^{1}	94.136 ± 0.077^{efgh}	-0.518 ± 0.013^{cdef}	6.148 ± 0.039^{c}	1.834 ± 0.053^{c}	0.000 ± 0.002^{a}	0.124 ± 0.006^{a}
CT^{5}M^{3}	93.643 ± 0.101^{ab}	-0.608 ± 0.039^{abcd}	6.992 ± 0.280^{de}	2.780 ± 0.294^{efg}	0.002 ± 0.002^{a}	0.124 ± 0.003^{a}
CT^{5}M^{5}	93.950 ± 0.174^{cdef}	-0.566 ± 0.023^{bcde}	6.202 ± 0.233^{c}	1.937 ± 0.268^{cd}	0.001 ± 0.002^{a}	0.120 ± 0.005^{a}

Values are expressed as mean ± standard deviation (n = 3). Different superscript letters within the same column indicate statistically significant differences ($p < 0.05$) by Duncan's multiple range test.

4) Tensile properties of bilayer films

The mechanical properties of the CT^1M^3/L^7B^3 bilayer film, composed of CT^1M^3 and L^7B^3 films exhibiting mechanically comparable characteristics, are summarized in Table 6. The CT^1M^3/L^7B^3 bilayer film exhibited a tensile strength of 33.15 ± 3.98 MPa, which was not significantly different from that of the CT^1M^3 monolayer film (34.44 ± 1.22 MPa) ($p > 0.05$). Similarly, the elongation at break of the CT^1M^3 film was 17.74 ± 1.96%, showing no statistically significant difference compared to that of the CT^1M^3/L^7B^3 bilayer film (18.60 ± 5.06%) ($p > 0.05$). These results suggest that the tensile deformation and fracture behavior of the laminated structure are predominantly governed by the brittle CT^1M^3 layer. During tensile loading, failure is initiated in the CT^1M^3 layer, which fractures first and consequently limits the overall extensibility of the bilayer film. In other words, although the ductile PBAT-containing L^7B^3 layer is incorporated into the laminated structure, the initial fracture occurs in the CT^1M^3 layer. Therefore, the bilayer design contributes more to enhancing structural integrity and barrier performance rather than significantly improving elongation behavior (90). In conclusion, the CT^1M^3/L^7B^3 bilayer film successfully maintained the mechanical strength of the CT^1M^3 monolayer film while achieving improved overall structural integrity and stability through the laminated configuration.

Table 6. Tensile properties of PLA, PBAT, PLA/PBAT blend (LB) films, CT^1M^3, and the laminated CT^1M^3/L^7B^3 bilayer film.

Sample	Tensile strength(Mpa)	Elastic modulus(Mpa)	Elongation at break(%)
PLA	33.09±0.22^{c}	2028.07±114.84^{e}	5.12±0.92^{a}
L^9B^1	39.28±0.13^{d}	2208.69±274.22^{e}	11.63±9.21^{a}
L^8B^2	35.47±1.07^{cd}	1897.19±663.22^{e}	42.51±13.94^{a}
L^7B^3	24.48±1.59^{b}	1450.71±179.30^{d}	33.58±15.20^{a}
L^6B^4	14.26±0.41^{a}	679.03±44.58^{c}	24.99±3.47^{a}
L^5B^5	13.22±1.40^{a}	566.97±42.90^{bc}	12.87±1.41^{a}
L^4B^6	16.34±0.66^{a}	697.87±124.81^{c}	25.85±7.13^{a}
L^3B^7	13.42±0.89^{a}	243.91±32.55^{ab}	38.95±8.64^{a}
L^2B^8	12.41±0.41^{a}	137.29±10.86^{a}	212.10±66.21^{b}
L^1B^9	14.05±1.45^{a}	104.22±3.43^{a}	324.33±88.83^{c}
PBAT	13.99±2.65^{a}	76.05±3.36^{a}	386.69±180.58^{c}
CT^1M^3	34.44±1.22^{c}	1201.76±18.81^{d}	17.74±1.96^{a}
CT^1M^3/L^7B^3	33.15±3.98^{c}	1114.82±2.08^{d}	18.60±5.06^{a}

Different superscript letters within the same column indicate statistically significant differences ($p < 0.05$) by Duncan's multiple range test.

4. Structural and chemical characterization of composite and bilayer films (XRD and FTIR)

1) X-ray diffraction (XRD) analysis

Figure 3 (a) presents the XRD patterns of neat carrageenan film, carrageenan composite films, L^7B^3 film, and laminated films. A strong peak was observed at 2θ = 29.45° in the neat carrageenan film. This peak is attributed to KCl crystals, an inorganic salt impurity commonly present in commercially supplied κ-carrageenan (91). The L^7B^3 film exhibited a relatively broad but intense peak at 2θ = 16.7°, corresponding to the characteristic peak of the (200)/(110) crystalline plane reflection of PLA α-form (92). Additionally, a peak was observed at 2θ = 29.45°, which has been reported as the (216) crystalline plane reflection of PLA α-form (92). Although this peak appears relatively weak in melt-crystallized pure PLA films (92), it was more clearly observed in the L^7B^3 film prepared by the chloroform solution casting process in this study, attributed to higher crystallinity achieved through slow solvent evaporation and the nucleation effect of PBAT. These results are consistent with previous studies demonstrating that solution casting influences the crystal structure formation of PLA (93).

Changes in diffraction patterns were observed as MCC and TiO_2 were incorporated into the carrageenan matrix. The intensity of the peak at 2θ = 29.45° in the CM^3 film decreased compared to the neat carrageenan film. This reduction suggests that MCC particles interfere with the regular arrangement and crystal growth of KCl. Despite the addition of MCC, characteristic peaks of cellulose I were not detected in the composite films. The strong diffraction peaks of the carrageenan matrix mask the relatively weak peaks of MCC present at low concentrations. A similar phenomenon has been reported in previous carrageenan/cellulose composite film studies (71).

The CT^1 film exhibited two notable features. The peak at 2θ = 29.45° was still present but with reduced intensity. A new distinct peak appeared at 2θ = 25.4°. This

additional peak corresponds to the (101) crystalline plane of anatase TiO_2 (94). This confirms that TiO_2 nanoparticles maintain their crystalline phase within the film matrix. The presence of this peak indicates successful incorporation of TiO_2 and preservation of structural integrity during the film formation process.

The XRD pattern of the CT^1M^3 film simultaneously exhibited characteristics of both CM^3 and CT^1 films. The peak at $2\theta = 25.4°$ (TiO_2) was clearly observed. In contrast, the intensity of the peak at $2\theta = 29.45°$ (KCl) decreased more significantly than in either CM^3 or CT^1 films alone. This synergistic effect suggests that the combined presence of MCC and TiO_2 most effectively suppresses the growth and crystallization of KCl impurities. This mechanism is likely related to both MCC and TiO_2 particles disrupting the regular arrangement of KCl crystals through steric hindrance and interfacial interactions. This is similar to the plasticizer effect reported by Sun et al. (2018) in hydroxypropyl methylcellulose/κ-carrageenan films.

Both surfaces of the laminated film were analyzed by XRD. CT^1M^3-L^7B^3 represents the measurement from the CT^1M^3 layer surface, while L^7B^3-CT^1M^3 represents the measurement from the L^7B^3 layer surface. In both measurements, the XRD patterns exhibited characteristic peaks of both constituent layers. The PLA characteristic peak at $2\theta = 16.7°$, the TiO_2 peak at $2\theta = 25.4°$, and the overlapping peaks of KCl from the CT^1M^3 layer and PLA α-form from the L^7B^3 layer around $2\theta = 29.45°$ were all observed. The similar diffraction patterns observed on both surfaces indicate uniform structural distribution throughout the laminated film and excellent interlayer adhesion. Notably, the peak intensity at $2\theta = 29.45°$ remained suppressed on both surfaces, confirming that the lamination process effectively controlled KCl crystallization without disrupting the crystal structure of individual layers. The preservation of these characteristic peaks confirms that the lamination process maintained the structural integrity of both the carrageenan composite layer and the PLA/PBAT layer. The consistent XRD patterns observed on both surfaces and the reduction in KCl crystallinity suggest improved compatibility and molecular-level interactions between

the components, which may contribute to the enhanced mechanical and barrier properties of the multilayer film (95).

2) Fourier-transform infrared sprctroscopy (FTIR) analysis

Measurements were performed in the spectral range from 4000 cm^{-1} to 400 cm^{-1}, and the FTIR results are presented in Figure 3 (b). Several characteristic absorption bands were observed in the neat κ-carrageenan film. The band around 3300 cm^{-1} is attributed to O-H stretching vibration of hydroxyl groups, indicating the presence of strong hydrogen bonding within the carrageenan matrix (71). The peak around 2923 cm^{-1} corresponds to symmetric and asymmetric C-H stretching vibrations (71). The peak at 1654 cm^{-1} represents amide-I vibration (71). The peak around 1223 cm^{-1} indicates S=O symmetric vibration of the sulfate groups (SO_3^-) in κ-carrageenan (96). The peaks at 1156 cm^{-1} and 1028 cm^{-1} are characteristic bands of C-O stretching vibration of the sugar ring and glycosidic (C-O-C) bonds in carrageenan (96). The peak at 919 cm^{-1} is attributed to 3,6-anhydro-D-galactose (C-O-C) vibration. The peak at 843 cm^{-1} is attributed to D-galactose-4-sulfate (96).

The FTIR spectrum of the CM^3 film with added MCC exhibited a nearly identical pattern to the neat carrageenan film. The characteristic peaks of MCC overlapped with the strong absorption bands of carrageenan and were not clearly distinguishable. The FTIR spectrum of the CT^1 film with added TiO_2 also showed a similar pattern to the neat carrageenan film. This is attributed to the strong absorption of the neat carrageenan matrix and the low TiO_2 content (94). The CT^1M^3 film also exhibited overlapping with the strong absorption bands of the carrageenan matrix.

In the FTIR spectrum of the L^7B^3 film, the peak at 1752 cm^{-1} is attributed to the ester carbonyl (C=O) stretching vibration of PLA (97). The O-H band at 3310 cm^{-1} observed in carrageenan films was barely detected in the L^7B^3 film, indicating the hydrophobic characteristics of the L^7B^3 film (97). The spectrum of the laminated film exhibited characteristic peaks from both layers. The O-H band at 3310 cm^{-1} and the

sulfate group peak at 1223 cm^{-1} from the carrageenan layer, as well as the C=O peak at 1752 cm^{-1} from the L^7B^3 film, were simultaneously observed (96). No new peaks appeared due to the bonding of the two layers, indicating that physical adhesion occurred without chemical reactions during the lamination process.

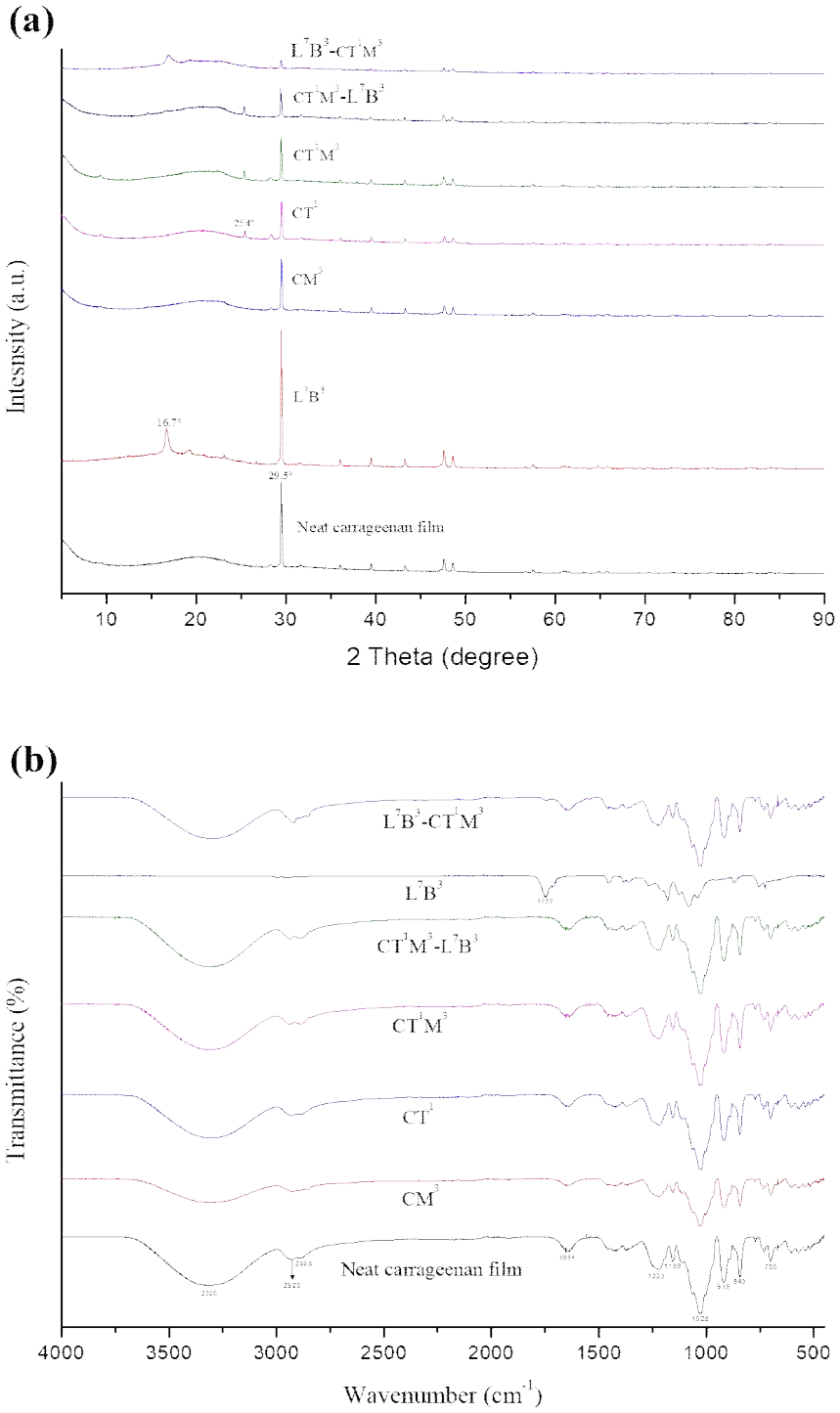


fig 3. XRD patterns (a) and FTIR spectra (b) of neat carrageenan film, carrageenan-based composite films, L^7B^3 film, and laminated CT^1M^3/L^7B^3 films.

5. Food application test: lipid oxidation stability assessed by peroxide value (POV)

This study evaluated the inhibitory effects of various film systems on lipid oxidation in sunflower oil, including an Blank, a positive control, CT^1, CM^3, CT^1M^3, and a CTM/LB film, using peroxide value (POV) as the primary indicator. POV is a widely accepted index of lipid oxidation that reflects the accumulation of primary lipid oxidation products, namely hydroperoxides, formed during storage and is commonly used to assess the freshness and oxidative stability of edible oils (98). In general, oils with a higher degree of unsaturation are more susceptible to oxidation, as oxygen readily reacts at double-bond sites to form lipid hydroperoxides, and these changes are sensitively reflected in POV values (99). The changes in POV for each film treatment over the storage period are presented in Figure 4. Under ambient storage conditions (0−70 days), POV increased continuously in all treatments, indicating progressive lipid oxidation in sunflower oil. The Blank exhibited the highest POV throughout the entire storage period, demonstrating the most rapid oxidation, while the neat carrageenan film showed slightly lower values than Blank but still maintained relatively high POV levels, indicating limited oxidation inhibition. This trend is consistent with previous studies reporting that the oxidative stability of sunflower oil varies significantly depending on packaging materials and storage conditions, such as exposure to oxygen and light (100). In contrast, the Positive group and CTM films containing TiO_2 and/or MCC exhibited intermediate POV levels, whereas the CTM/LB film maintained the lowest or near-lowest POV after day 3 of storage across most time points. Meanwhile, oxygen transmission rate (OTR) measurements (Table 4) showed that CTM and CTM/LB films had significantly lower oxygen permeability than the neat carrageenan film ($p < 0.05$), exhibiting oxygen barrier performance comparable to that of the positive control. This enhanced oxygen barrier property is considered to play a key role in suppressing the increase in POV of sunflower oil, which is in agreement with previous reports

demonstrating that differences in packaging materials directly influence the formation of primary lipid oxidation products (hydroperoxides) as well as oxidation-related volatile compounds in edible oils (101). Therefore, the composite structure based on CTM film incorporating inorganic fillers and an LB layer shows strong potential as a packaging material capable of improving the oxidative stability of sunflower oil under ambient storage conditions, consistent with recent trends in carrageenan-based composite film for active and intelligent food packaging applications (47,102,103).

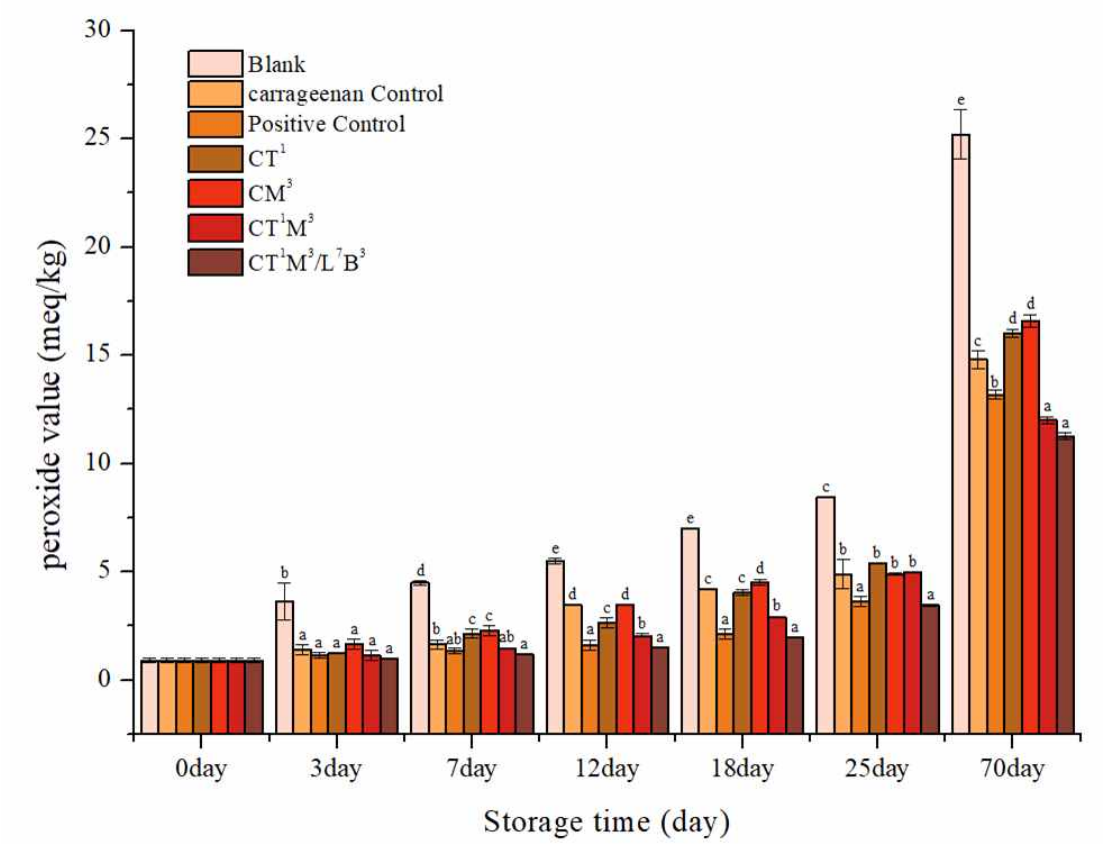


fig 4. Changes in peroxide value (POV) of sunflower oil during storage (0–70 days) under different film packaging systems.

6. Lipid oxidation kinetics

To quantitatively evaluate the oxidative stability of sunflower oil packaged with various films during storage, peroxide values (POV) were measured at 25°C over storage periods of 0, 3, 7, 12, 18, 25, and 70 days. The data were modeled using both zero-order kinetics (POV = a + k·t) and pseudo-first-order kinetics (ln(POV) = ln(a) + k·t). The zero-order kinetic model consistently exhibited superior fit across all film conditions, as evidenced by higher R^2 values, and the corresponding kinetic parameters are presented in Table 7. The linear increase in peroxide value over the storage period suggests that lipid oxidation proceeded under diffusion-controlled conditions, where the reaction rate is primarily governed by oxygen diffusion. Similar zero-order kinetic behavior has been reported for oils stored in systems with headspace or semi-sealed configurations, where oxygen concentration in the headspace remains relatively constant during the initial stages of oxidation (104,105,106,107). The experimental setup employed in this study, consisting of vials with limited headspace sealed with barrier films and stored isothermally at 25°C, can be considered an oxygen-limited environment, which accounts for the nearly linear increase in POV over time. The rate constant (k) represents a quantitative parameter describing the accumulation rate of peroxides, the primary oxidation products, and serves as a direct indicator of lipid oxidation progression. Therefore, k values can be utilized as a reliable quantitative metric for comparing lipid oxidation inhibition efficiency among different film formulations (107,108). The unpackaged blank exhibited the highest k value of 0.33 ± 0.02 meq O_2 /kg·day, indicating the most rapid oxidation progression. When oil was packaged with neat carrageenan film, the k value decreased to 0.20 ± 0.01 meq O_2 /kg·day, representing an approximately 39% reduction compared to the blank. The positive control film demonstrated a further reduction in k value to 0.18 ± 0.00 meq O_2 /kg·day, corresponding to an approximately 45% decrease. CT[1] and CM[3] exhibited intermediate k values of 0.22 ± 0.00 meq O_2 /kg·day, which were significantly lower than the blank but higher than

the positive control ($p < 0.05$). The optimized CT^1M^3 film exhibited a lower k value of 0.16 ± 0.00 meq O_2 /kg·day, while the CT^1M^3/L^7B^3 bilayer film demonstrated the lowest k value of 0.15 ± 0.00 meq O_2 /kg·day among all experimental groups ($p < 0.05$). This represents an approximately 55% reduction compared to the blank and is lower than the positive control, confirming lipid oxidation inhibition performance equivalent to or exceeding that of commercial high-barrier films. These results can be attributed to the synergistic effect of the excellent oxygen barrier properties of the CT^1M^3 layer and the water vapor barrier properties of the L^7B^3 layer, which effectively suppressed lipid oxidation induced by both oxygen and moisture. In summary, zero-order kinetic analysis demonstrated that the oxygen barrier properties of films directly influence the rate of lipid oxidation. In particular, the CT^1M^3/L^7B^3 bilayer film exhibited the lowest rate constant among all experimental groups, confirming its potential as an effective packaging material for enhancing the oxidative stability of oxygen-sensitive foods (109,110).

Table 7. Zero-order and pseudo-first-order kinetic parameters of lipid oxidation (k, a, R^2, RMSE and AIC) for oil samples packaged with neat carrageenan and carrageenan/TiO_2 /MCC-based films.

Films	Zero-order kinetics					Pseudo-first-order kinetics				
	[a]K	[b]a	[c]R^2	[d]RMSE	[e]AIC	K	a	R^2	RMSE	AIC
blank	0.33 ± 0.02[e]	1.48 ± 0.32[c]	0.99 ± 0.01[b]	0.83 ± 0.22[c]	1.10 ± 4.00[c]	0.04 ± 0.00[a]	0.99 ± 0.07[e]	0.75 ± 0.03[a]	0.46 ± 0.01[d]	-6.92 ± 0.39[d]
Neat carrageena	0.20 ± 0.01[c]	0.64 ± 0.26[b]	0.99 ± 0.01[b]	0.42 ± 0.27[a]	-9.82 ± 8.41[a]	0.04 ± 0.00[a]	0.41 ± 0.10[cd]	0.86 ± 0.01[b]	0.32 ± 0.02[c]	-11.90 ± 1.05[c]
positive control	0.18 ± 0.00[b]	-0.04 ± 0.11[a]	0.96 ± 0.01[a]	0.76 ± 0.05[bc]	0.13 ± 0.83[c]	0.04 ± 0.00[a]	0.06 ± 0.08[a]	0.97 ± 0.01[d]	0.14 ± 0.03[a]	-23.75 ± 2.77[a]
CT^1	0.22 ± 0.00[d]	0.42 ± 0.09[b]	0.99 ± 0.00[b]	0.39 ± 0.07[a]	-9.21 ± 2.49[a]	0.04 ± 0.00[a]	0.39 ± 0.03[c]	0.89 ± 0.01[c]	0.29 ± 0.01[bc]	-13.36 ± 0.55[bc]
CM^3	0.22 ± 0.00[d]	0.64 ± 0.09[b]	0.99 ± 0.00[b]	0.56 ± 0.06[ab]	-4.14 ± 1.50[ab]	0.04 ± 0.00[a]	0.52 ± 0.06[d]	0.88 ± 0.00[bc]	0.30 ± 0.00[c]	-13.05 ± 0.18[bc]
CT^1M^3	0.16 ± 0.00[a]	0.49 ± 0.05[b]	0.99 ± 0.00[b]	0.37 ± 0.05[a]	-10.07 ± 1.84[a]	0.04 ± 0.00[a]	0.22 ± 0.05[b]	0.90 ± 0.01[c]	0.26 ± 0.03[b]	-14.84 ± 1.41[b]
CT^1M^3/ L^7B^3	0.15 ± 0.00[a]	0.09 ± 0.02[a]	0.97 ± 0.00[a]	0.59 ± 0.02[abc]	-3.48 ± 0.45[ab]	0.04 ± 0.00[a]	0.00 ± 0.00[a]	0.97 ± 0.00[d]	0.15 ± 0.00[a]	-22.96 ± 0.34[a]

Results are presented as means ± standard deviation. Values with the different superscript letters in the same column indicate that they are statistically different ($p < 0.05$).

[a]k: rate constant (zero-order: meq O2/kg·day; first-order: day−1).

[b]a: intercept (zero-order: meq O2/kg; first-order: dimensionless).

[c]R2: coefficient of determination.

[d]RMSE: root mean square error (meq O2/kg).

[e]AIC: Akaike information criterion.

CHAPTER 4 Conclusion

In this study, biodegradable κ-carrageenan-based composite laminate films with enhanced barrier properties were developed for food packaging applications. The CT^1M^3 composite film containing 1 wt% TiO_2 and 3 wt% MCC exhibited an 88.5% reduction in oxygen permeability (OP) compared to the neat carrageenan film. To compensate for the high water vapor permeability (WVP) inherent to hydrophilic carrageenan, a bilayer structure was fabricated by laminating CT^1M^3 with a PLA/PBAT (7:3) blend film. The resulting CT^1M^3/L^7B^3 bilayer film achieved a 98.9% reduction in water vapor permeability while maintaining oxygen barrier performance comparable to that of commercial high-barrier films. Furthermore, the CT^1M^3/L^7B^3 film exhibited transmittance values of 0.001% at 280 nm and 0.56% at 660 nm, demonstrating excellent light-blocking performance in both the UV and visible light regions. Kinetic analysis based on peroxide value (POV) measurements during sunflower oil storage revealed that lipid oxidation followed zero-order kinetics, with the CT^1M^3/L^7B^3 film exhibiting the lowest oxidation rate constant (k) among all tested samples. These results suggest that the developed CT^1M^3/L^7B^3 film has potential as a biodegradable packaging material for food products requiring high barrier properties. Moreover, since all constituent materials are biodegradable, the developed multilayer film is expected to serve as an eco-friendly alternative to conventional petroleum-based high-barrier films.

References

1. Amin U, Khan MKI, Maan AA, Nazir A, Riaz S, Khan MU, Sultan M, Munekata PES, Lorenzo JM. Biodegradable active, intelligent, and smart packaging materials for food applications. Food Packaging and Shelf Life 33, 100903 (2022)

2. Ahmed MW, Haque MA, Mohibbullah M, Khan MSI, Islam MA, Mondal MHT, Ahmmed R. A review on active packaging for quality and safety of foods: Current trends, applications, prospects and challenges. Food Packaging and Shelf Life 33, 100913 (2022)

3. Geng L, Liu K, Zhang H. Lipid oxidation in foods and its implications on proteins. Frontiers in Nutrition 10, 1192199 (2023)

4. Abeyrathne EDNS, Nam K, Ahn DU. Analytical methods for lipid oxidation and antioxidant capacity in food systems. Antioxidants 10(10), 1587 (2021)

5. Clarke HJ, McCarthy WP, O'Sullivan MG, Kerry JP, Kilcawley KN. Oxidative quality of dairy powders: Influencing factors and analysis. Foods 10(10), 2315 (2021)

6. Yao L, Sun H, Yu C, Weng Y. Enhanced Xylan/PVA Composite Films via Nano-ZnO Reinforcement for Sustainable Food Packaging. Polymers 17(8), 1080 (2025)

7. Barbato A, Apicella A, Malvano F, Scarfato P, Incarnato L. High-barrier, biodegradable films with polyvinyl alcohol/polylactic acid+ wax double coatings: influence of relative humidity on transport properties and suitability for modified atmosphere packaging applications. Polymers 15(19), 4002 (2023)

8. Huang HD, Ren PG, Zhong GJ, Olah A, Li ZM, Baer E, Zhu L. Promising strategies and new opportunities for high barrier polymer packaging films. Progress

in Polymer Science 144, 101722 (2023)

9. Yuan S, Zhang S, Pei L, Liu Y, Sun Y, Peng J, Wang H. Elaborating conspicuously low hydrogen permeability EVOH composite membrane upgraded by corrosion protection function. Journal of Membrane Science 708, 123050 (2024)

10. Baddigam KR, Chee BS, Guilloud E, Venkatesh C, Koninckx H, Windey K, Svagan AJ. High oxygen barrier packaging materials from protein-rich single-celled organisms. Communications Chemistry 8(1), 297 (2025)

11. Yue S, Zhang T, Wang S, Han D, Huang S, Xiao M, Meng Y. Recent progress of biodegradable polymer package materials: nanotechnology improving both oxygen and water vapor barrier performance. Nanomaterials 14(4), 338 (2024)

12. Mujtaba M, Lipponen J, Ojanen M, Puttonen S, Vaittinen H. Trends and challenges in the development of bio-based barrier coating materials for paper/cardboard food packaging; a review. Science of the total environment 851, 158328 (2022)

13. Türksever C, Koç B, Kizilirmak Esmer O. Sustainable Alternatives in Multilayer Packaging: Storage Stability of Pudding Powder Under Accelerated Storage Conditions. Foods 14(22), 3806 (2025)

14. Bauer AS, Tacker M, Uysal-Unalan I, Cruz RM, Varzakas T, Krauter V. Recyclability and redesign challenges in multilayer flexible food packaging—A review. Foods 10(11), 2702 (2021)

15. Patel J, Parhi A, Al-Ghamdi S, Sonar CR, Mattinson DS, Tang J, Sablani SS. Stability of vitamin C, color, and garlic aroma of garlic mashed potatoes in polymer packages processed with microwave-assisted thermal sterilization technology. Journal of Food Science 85(9), 2843-2851 (2020)

16. Jiao H, Ali SS, Alsharbaty MHM, Elsamahy T, Abdelkarim E, Schagerl M, Sun

JA. critical review on plastic waste life cycle assessment and management: Challenges, research gaps, and future perspectives. Ecotoxicology and Environmental Safety 271, 115942 (2024)

17. Najahi H, Banni M, Nakad M, Abboud R, Assaf JC, Operato L, Hamd W. Plastic pollution in food packaging systems: impact on human health, socioeconomic considerations and regulatory framework. Journal of Hazardous Materials Advances 18, 100667 (2025)

18. Operato L, Panzeri A, Masoero G, Gallo A, Gomes L, Hamd W. Food packaging use and post-consumer plastic waste management: a comprehensive review. Frontiers in Food Science and Technology 5, 1520532 (2025)

19. Schmidt J, Grau L, Auer M, Maletz R, Woidasky J. Multilayer packaging in a circular economy. Polymers 14(9), 1825 (2022)

20. Lewanska M, Barczynska R. Microplastics from Food Packaging: Polymer Degradation Pathways, Environmental Distribution, and Effects on the Human Gastrointestinal Tract. Polymers 17(21), 2923 (2025)

21. Pilevar Z, Bahrami A, Beikzadeh S, Hosseini H, Jafari SM. Migration of styrene monomer from polystyrene packaging materials into foods: Characterization and safety evaluation. Trends in Food Science & Technology 91, 248-261 (2019)

22. Gerassimidou S, Geueke B, Groh KJ, Muncke J, Hahladakis JN, Martin OV, Iacovidou E. Unpacking the complexity of the polyethylene food contact articles value chain: A chemicals perspective. Journal of Hazardous Materials 454, 131422 (2023)

23. Li T, Theodosopoulos G, Lovell C, Loukodimou A, Maniam KK, Paul S. Progress in solvent-based recycling of polymers from multilayer packaging. Polymers 16(12), 1670 (2024)

24. Walker TW, Frelka N, Shen Z, Chew AK, Banick J, Grey S, Huber GW. Recycling of multilayer plastic packaging materials by solvent-targeted recovery and precipitation. Science advances 6(47), 7599 (2020)

25. Jakobs M, Kroell N. Influence of plastic packaging design on the sensor-based sortability in lightweight packaging waste sorting plants. Resources, Conservation and Recycling 207, 107599 (2024)

26. Li K, Du L, Qin C, Bolan N, Wang H, Wang H. Microplastic pollution as an environmental risk exacerbating the greenhouse effect and climate change: a review. Carbon Research 3(1), 9 (2024)

27. OECD: ORGANISATION FOR ECONOMIC CO-OPERATION AND DEVELOPMENT. Policy scenarios for eliminating plastic pollution by 2040 (2024)

28. Xia C, Cai L, Lam SS, Sonne C. Microplastics pollution: Economic loss and actions needed. Eco-Environment & Health 2(2), 41-42 (2023)

29. Ceballos-Santos S, de Sousa DB, García PG, Laso J, Margallo M, Aldaco R. Exploring the environmental impacts of plastic packaging: A comprehensive life cycle analysis for seafood distribution crates. Science of the Total Environment 951, 175452 (2024)

30. Villarrubia-Gómez P, Almroth BC, Eriksen M, Ryberg M, Cornell SE. Plastics pollution exacerbates the impacts of all planetary boundaries. One Earth 7(12), 2119-2138 (2024)

31. European Commission: A European Strategy for Plastics in a Circular Economy. Final Report of European Commission, EU-EC-2018-PLASTICS-STRATEGY (2018)

32. El-Sayed SM, Youssef AM. Eco-friendly biodegradable nanocomposite materials

and their recent use in food packaging applications: a review. Sustainable Food Technology 1(2), 215-227 (2023)

33. Westlake JR, Tran MW, Jiang Y, Zhang X, Burrows AD, Xie M. Biodegradable biopolymers for active packaging: demand, development and directions. Sustainable Food Technology 1(1), 50-72 (2023)

34. Shaikh S, Yaqoob M, Aggarwal P. An overview of biodegradable packaging in food industry. Current research in food science 4, 503-520 (2021)

35. Upadhyay P, Zubair M, Roopesh MS, Ullah A. An overview of advanced antimicrobial food packaging: emphasizing antimicrobial agents and polymer-based films. Polymers 16(14), 2007 (2024)

36. Periyasamy T, Asrafali SP, Lee J. Recent Advances in Functional Biopolymer Films with Antimicrobial and Antioxidant Properties for Enhanced Food Packaging. Polymers 17(9), 1257 (2025)

37. Esfandiari Z, Hassani B, Sani IK, Talebi A, Mohammadi F, Zomorodi S, Jafari SM. Characterization of edible films made with plant carbohydrates for food packaging: A comprehensive review. Carbohydrate Polymer Technologies and Applications 11, 100979 (2025)

38. Junaid PM, Saikumar A, Islam RU, Patel MK, Eranda DHU, Islam M, Badwaik LS. Polysaccharide-based biopolymers: exploring film fabrication techniques, molecular interactions, and their potential food applications. Quality Assurance and Safety of Crops & Foods 17(4), 257-283 (2025)

39. Pires AF, Díaz O, Cobos A, Pereira CDA. review of recent developments in edible films and coatings-focus on whey-based materials. Foods 13(16), 2638 (2024)

40. Schenk S, Bucher M, Herrenbauer M, Schmid D, Schmid M. Challenges of

Alginate-Based Cast Films in Plastic-Free Food Packaging Applications: An Overview. Polymers 17(22), 3061 (2025)

41. Biratu G, Woldemariam HW, Gonfa G. Development of active edible films from coffee pulp pectin, propolis, and honey with improved mechanical, functional, antioxidant, and antimicrobial properties. Carbohydrate Polymer Technologies and Applications 8, 100557 (2024)

42. Eslami Z, Elkoun S, Robert M, Adjallé K. A review of the effect of plasticizers on the physical and mechanical properties of alginate-based films. Molecules 28(18), 6637 (2023)

43. Romruen O, Kaewprachu P, Sai-Ut S, Kingwascharapong P, Karbowiak T, Zhang W, Rawdkuen S. Impact of environmental storage conditions on properties and stability of a smart bilayer film. Scientific Reports 14(1), 23038 (2024)

44. Riahi Z, Khan A, Rhim JW, Shin GH, Kim JT. Sustainable packaging film based on cellulose nanofibres/pullulan impregnated with zinc-doped carbon dots derived from avocado peel to extend the shelf life of chicken and tofu. International Journal of Biological Macromolecules 258, 129302 (2024)

45. Ghosh T, Priyadarshi R, de Souza CK, Angioletti BL, Rhim JW. Advances in pullulan utilization for sustainable applications in food packaging and preservation: A mini-review. Trends in food science & technology 125, 43-53 (2022)

46. Rashid A, Qayum A, Liang Q, Kang L, Ekumah JN, Han X, Ma H. Exploring the potential of pullulan-based films and coatings for effective food preservation: A comprehensive analysis of properties, activation strategies and applications. International Journal of Biological Macromolecules 260, 129479 (2024)

47. Kokkuvayil Ramadas B, Rhim JW, Roy S. Recent progress of carrageenan-based

composite films in active and intelligent food packaging applications. Polymers 16(7), 1001 (2024)

48. Roy S, Rhim JW. Carrageenan/agar-based functional film integrated with zinc sulfide nanoparticles and Pickering emulsion of tea tree essential oil for active packaging applications. International Journal of Biological Macromolecules 193, 2038-2046 (2021)

49. Wang R, Zhang S, Liu S, Sun Y, Xu H. A contribution to improve barrier properties and reduce swelling ratio of κ-carrageenan film from the incorporation of guar gum or locust bean gum. Polymers 15(7), 1751 (2023)

50. Mavelil-Sam R, Ouseph EM, Morreale M, Scaffaro R, Thomas S. Recent Developments and Formulations for Hydrophobic Modification of Carrageenan Bionanocomposites. Polymers 15, 1650 (2023)

51. Sharafi Zamir S, Fathi B, Ajji A, Robert M, Elkoun S. Crystallinity and gas permeability of poly (lactic acid)/starch nanocrystal nanocomposite. Polymers 14(14), 2802 (2022)

52. Phothisarattana D, Wongphan P, Promhuad K, Promsorn J, Harnkarnsujarit N. Biodegradable poly (butylene adipate-co-terephthalate) and thermoplastic starch-blended TiO2 nanocomposite blown films as functional active packaging of fresh fruit. Polymers 13(23), 4192 (2021)

53. Pietrosanto A, Scarfato P, Di Maio L, Incarnato L. Development of PLA/PHB blown films with improved performance for food packaging applications. Chemical Engineering Transactions 87, 91-96 (2021)

54. Shi K, Liu G, Sun H, Weng Y. Polylactic acid/lignin composites: A review. Polymers 15(13), 2807 (2023)

55. Venkatesan R, Alagumalai K, Vetcher AA, Al-Asbahi BA, Kim SC. Eco-friendly

poly (butylene adipate-co-terephthalate) coated bi-layered films: an approach to enhance mechanical and barrier properties. Polymers 16(9), 1283 (2024)

56. Roy S, Ghosh T, Zhang W, Rhim JW. Recent progress in PBAT-based films and food packaging applications: A mini-review. Food Chemistry 437, 137822 (2024)

57. Martins VF, Pintado ME, Morais RM, Morais AM. Recent highlights in sustainable bio-based edible films and coatings for fruit and vegetable applications. Foods 13(2), 318 (2024)

58. Zhao Y, Li B, Li C, Xu Y, Luo Y, Liang D, Huang C. Comprehensive review of polysaccharide-based materials in edible packaging: A sustainable approach. Foods 10(8), 1845 (2021)

59. Xie F. Biopolymer-based multilayer films and coatings for food preservation: An update of the recent development. Current Food Science and Technology Reports 1(1), 1-12 (2023)

60. Li Y, Ren J, Wang B, Lu W, Wang H, Hou W. Development of biobased multilayer films with improved compatibility between polylactic acid-chitosan as a function of transition coating of SiOx. International Journal of Biological Macromolecules 165, 1258-1263 (2020)

61. Wang Q, Chen W, Zhu W, McClements DJ, Liu X, Liu F. A review of multilayer and composite films and coatings for active biodegradable packaging. npj Science of Food 6(1), 18 (2022)

62. Alias A.R, Wan MK, Sarbon NM. Emerging materials and technologies of multi-layer film for food packaging application: A review. Food Control 136, 108875 (2022)

63. Pasquier E, Mattos BD, Koivula H, Khakalo A, Belgacem MN, Rojas OJ, Bras

J. Multilayers of renewable nanostructured materials with high oxygen and water vapor barriers for food packaging ACS Applied Materials & Interfaces, 14(26), 30236-30245 (2022)

64. Tedeschi G, Guzman-Puyol S, Ceseracciu L, Benitez JJ, Cataldi P, Bissett M, Heredia-Guerrero JA. Sustainable, high-barrier polyaleuritate/nanocellulose biocomposites. ACS Sustainable Chemistry & Engineering 8(29), 10682-10690 (2020)

65. Yuvaraj G, Ramesh M, Rajeshkumar L. Carbon and cellulose-based nanoparticle-reinforced polymer nanocomposites: a critical review. Nanomaterials 13(11), 1803 (2023)

66. Tayeb A, Tajvidi M, Bousfield D. Enhancing the oxygen barrier properties of nanocellulose at high humidity: numerical and experimental assessment. Sustainable Chemistry 1(3), 14 (2020)

67. Lee SJ, Yoon SJ, Jeon IY. Graphene/polymer nanocomposites: Preparation, mechanical properties, and application. Polymers 14(21), 4733 (2022)

68. Pulikkalparambil H, Phothisarattana D, Promhuad K, Harnkarnsujarit N. Effect of silicon dioxide nanoparticle on microstructure, mechanical and barrier properties of biodegradable PBAT/PBS food packaging. Food Bioscience 55, 103023 (2023).

69. Chen Q, Shi Y, Chen G, Cai M. Enhanced mechanical and hydrophobic properties of composite cassava starch films with stearic acid modified MCC (microcrystalline cellulose)/NCC (nanocellulose) as strength agent. International journal of biological macromolecules 142, 846-854 (2020)

70. Emenike EC, Iwuozor KO, Saliu OD, Ramontja J, Adeniyi AG. Advances in the extraction, classification, modification, emerging and advanced applications of crystalline cellulose: a review. Carbohydrate Polymer Technologies and

Applications 6, 100337 (2023)

71. Park SY, Kim HL, Her JY. Isolation of microcrystalline cellulose (MCC) from pistachio shells and preparation of carrageenan-based composite films. Carbohydrate Polymer Technologies and Applications 7, 100423 (2024)

72. Hamdan MA, Ramli NA, Othman NA, Amin KNM, Adam F. Characterization and property investigation of microcrystalline cellulose (MCC) and carboxymethyl cellulose (CMC) filler on the carrageenan-based biocomposite film. Materials Today: Proceedings 42, 56-62 (2021)

73. Phothisarattana D, Harnkarnsujarit N. Migration, aggregations and thermal degradation behaviors of TiO2 and ZnO incorporated PBAT/TPS nanocomposite blown films. Food Packaging and Shelf Life 33, 100901 (2022)

74. Zhang W, Rhim JW. Titanium dioxide (TiO2) for the manufacture of multifunctional active food packaging films. Food Packaging and Shelf Life 31, 100806 (2022)

75. Shaili T, Abdorreza MN, Fariborz N. Functional, thermal, and antimicrobial properties of soluble soybean polysaccharide biocomposites reinforced by nano TiO2. Carbohydrate Polymers 134, 726-731 (2015)

76. Phothisarattana D, Wongphan P, Promhuad K, Promsorn J, Harnkarnsujarit N. Biodegradable poly (butylene adipate-co-terephthalate) and thermoplastic starch-blended TiO2 nanocomposite blown films as functional active packaging of fresh fruit. Polymers 13(23), 4192 (2021)

77. Zhu Y, Wang T, Dai Y, Wang Y, Ding Y, Zhang L. Surface engineering of regenerated cellulose nanocomposite films with high strength, ultraviolet resistance, and a hydrophobic surface. Polymers 15(6), 1427 (2023)

78. Peng S, Zhu Z, Wei Y. An analytic solution for bending of multilayered

structures with interlayer-slip. International Journal of Mechanical Sciences 282, 109642 (2024)

79. Shao Y, Yan J, Zhi Y, Li C, Li Q, Wang K, Yu Y. A universal packaging substrate for mechanically stable assembly of stretchable electronics. Nature Communications 15(1), 6106 (2024)

80. Lang F, Zhou Z, Liu J, Cui M, Zhang Z. Review on the impact of marine environment on the reliability of electronic packaging materials. Frontiers in Materials 12, 1584349 (2025)

81. Lee JS, Lee ES, Han J. Enhancement of the water-resistance properties of an edible film prepared from mung bean starch via the incorporation of sunflower seed oil. Scientific reports 10(1), 13622 (2020)

82. Janik W, Nowotarski M, Shyntum DY, Banaś A, Krukiewicz K, Kudła S, Dudek G. Antibacterial and biodegradable polysaccharide-based films for food packaging applications: Comparative study. Materials 15(9), 3236 (2022)

83. Deng Y, Yu C, Wongwiwattana P, Thomas NL. Optimising ductility of poly (lactic acid)/poly (butylene adipate-co-terephthalate) blends through co-continuous phase morphology. Journal of Polymers and the Environment 26(9), 3802-3816 (2018)

84. Coiai S, Di Lorenzo ML, Cinelli P, Righetti MC, Passaglia E. Binary Green Blends of Poly (lactic acid) with Poly (butylene adipate-co-butylene terephthalate) and Poly (butylene succinate-co-butylene adipate) and Their Nanocomposites. Polymers 13(15), 2489 (2021)

85. Rhim JW, Mohanty KA, Singh SP, Ng PK. Preparation and properties of biodegradable multilayer films based on soy protein isolate and poly (lactide). Industrial & engineering chemistry research 45(9), 3059-3066 (2006)

86. Valdés A, Martínez C, Garrigos MC, Jimenez A. Multilayer films based on poly (lactic acid)/gelatin supplemented with cellulose nanocrystals and antioxidant extract from almond shell by-product and its application on hass avocado preservation. Polymers 13(21), 3615 (2021)

87. Hosseini SF, Javidi Z, Rezaei M. Efficient gas barrier properties of multi-layer films based on poly (lactic acid) and fish gelatin. International Journal of Biological Macromolecules 92, 1205-1214 (2016)

88. Sedayu BB, Cran MJ, Bigger SW. A review of property enhancement techniques for carrageenan-based films and coatings. Carbohydrate polymers 216, 287-302 (2019)

89. Sun J, Yang X, Bai Y, Fang Z, Zhang S, Wang X, Guo Y. Recent advances in cellulose nanofiber modification and characterization and cellulose nanofiber-based films for eco-friendly active food packaging. Foods 13(24), 3999 (2024)

90. Ponnusamy A, Palamae S, Prodpran T, Kim JT, Zhang B, Ma L, Benjakul S. Fabrication of a Chitosan−Gelatin/Polylactic Acid Bilayer Active Film Loaded with Tannic Acid for Enhancing Shelf-Life of Refrigerated Baby Clams. Foods 14(22), 3934 (2025)

91. Sun G, Liang T, Tan W, Wang L. Rheological behaviors and physical properties of plasticized hydrogel films developed from κ-carrageenan incorporating hydroxypropyl methylcellulose. Food Hydrocolloids 85, 61-68 (2018)

92. Puchalski M, Kwolek S, Szparaga G, Chrzanowski M, Krucińska I. Investigation of the influence of PLA molecular structure on the crystalline forms (α'and α) and mechanical properties of wet spinning fibres. Polymers 9(1), 18 (2017)

93. Huang R, Zhu X, Tu H, Wan A. The crystallization behavior of porous poly (lactic acid) prepared by modified solvent casting/particulate leaching technique

for potential use of tissue engineering scaffold. Materials letters 136, 126-129 (2014)

94. Hou X, Xue Z, Liu J, Yan M, Xia Y, Ma Z. Characterization and property investigation of novel eco‐friendly agar/carrageenan/TiO2 nanocomposite films. Journal of Applied Polymer Science 136(10), 47113 (2019)

95. Fu X, Chang X, Ding Z, Xu H, Kong H, Chen F, Ding S. Fabrication and characterization of eco-friendly polyelectrolyte bilayer films based on chitosan and different types of edible citrus pectin. Foods 11(21), 3536 (2022)

96. Pereira L, Amado AM, Critchley AT, Van de Velde F, Ribeiro-Claro PJ. Identification of selected seaweed polysaccharides (phycocolloids) by vibrational spectroscopy (FTIR-ATR and FT-Raman). Food hydrocolloids 23(7), 1903-1909 (2009)

97. Rhim JW. Effect of PLA lamination on performance characteristics of agar/κ-carrageenan/clay bio-nanocomposite film. Food Research International 51(2), 714-722 (2013)

98. Barriuso B, Astiasarán I, Ansorena D. A review of analytical methods measuring lipid oxidation status in foods: a challenging task. European food research and technology 236(1), 1-15 (2013)

99. Choe E, Min DB. Mechanisms and factors for edible oil oxidation. Comprehensive reviews in food science and food safety 5(4), 169-186 (2006)

100. Kucuk M, Caner C. Effect of packaging materials and storage conditions on sunflower oil quality. Journal of Food Lipids 12(3), 222-231 (2005)

101. Huyan Z, Ding S, Mao X, Wu C, Yu X. Effects of packaging materials on oxidative product formation in vegetable oils: Hydroperoxides and volatiles. Food Packaging and Shelf Life 21, 100328 (2019)

102. Cheng C, Chen S, Su J, Zhu M, Zhou M, Chen T, Han Y. Recent advances in carrageenan-based films for food packaging applications. Frontiers in Nutrition 9, 1004588 (2022)

103. Mathew SS, Jaiswal AK, Jaiswal S. Carrageenan-based sustainable biomaterials for intelligent food packaging: A review. Carbohydrate Polymers 342, 122267 (2024)

104. Tsao CH, Chang CW, Ho YC, Chuang YK, Lee WJ. Application of OXITEST for prediction of shelf-lives of selected cold-pressed oils. Frontiers in Nutrition 8, 763524 (2021)

105. Farhoosh R. Initiation and propagation kinetics of inhibited lipid peroxidation. Scientific Reports 11(1), 6864 (2021)

106. Khabbaz ES, Jaldani S, Farhoosh R. Unusual multiphase peroxidation of sunflower oil: A kinetic study. LWT 184, 114981 (2023)

107. Ghosh M, Upadhyay R, Mahato DK, Mishra HN. Kinetics of lipid oxidation in omega fatty acids rich blends of sunflower and sesame oils using Rancimat. Food chemistry 272, 471-477 (2019)

108. Farhoosh R, Niazmand R, Rezaei M, Sarabi M. Kinetic parameter determination of vegetable oil oxidation under Rancimat test conditions. European Journal of Lipid Science and Technology 110(6), 587-592 (2008)

109. Domínguez R, Pateiro M, Gagaoua M, Barba FJ, Zhang W, Lorenzo JM. A comprehensive review on lipid oxidation in meat and meat products. Antioxidants 8(10), 429 (2019)

110. Shahidi F, Zhong Y. Lipid oxidation and improving the oxidative stability. Chemical society reviews 39(11), 4067-4079 (2010)